Thesis for the degree of Doctor of Philosophy

Durability of Reinforced Concrete under Impressed Current Cathodic Protection

Failure Mechanism and Service Life Prediction

Emma Qingnan Zhang

Department of Architecture and Civil Engineering
CHALMERS UNIVERSITY OF TECHNOLOGY
Gothenburg, Sweden 2018

Durability of Reinforced Concrete under Impressed Current Cathodic Protection

Failure Mechanism and Service Life Prediction

Emma Qingnan Zhang

ISBN 978-91-7597-711-9

Doktorsavhandlingar vid Chalmers tekniska högskola

Ny serie nr 4392

ISSN 0346-718X

Department of Architecture and Civil Engineering

Chalmers University of Technology

SE–412 96 Gothenburg, Sweden

Telephone + 46 (0) 31 – 772 1000

Typeset by the author using LaTeX.

Printed by Chalmers Reproservice

Gothenburg, Sweden 2018

To Brook, Victoria

& my parents

Abstract

Impressed current cathodic protection (ICCP) and prevention (ICCPre) are reliable and efficient techniques to stop, control and postpone corrosion in reinforced concrete structures. However, the wide application of this technique has been limited by the high cost of the anode system. Moreover, the long-term electrochemical effects on the anode–concrete interface and the steel reinforcement are still not completely clear. These effects can be beneficial or unfavorable, which will influence the performance and service life of the structure. Therefore, the long-term electrochemical effects greatly need to be quantified and taken into consideration in durability design.

The present thesis has been devoted to gaining more solid scientific understanding into this issue through experimental work. A novel and affordable carbon fiber reinforced polymer (CFRP) mesh was used as anode material instead of traditional metallic anode. Accelerated tests, using relatively high current densities, were adopted to evaluate the long-term electrochemical effects. The impact of the accelerated tests was studied and modeled. Varied characterization and monitoring techniques were employed to analyze the anode–concrete interface and the steel condition as well as chloride content.

The results show that the CFRP meshes are suitable as anode material for cathodic prevention applications, with a service life of more than 100 years. Calcium leaching at the anode–concrete interface was inevitable as a consequence of chemical reactions and mass transport under current exchange. The chemical changes can cause material loss and increase the resistance of the concrete and eventually make the system fail. With low current densities, the chemical changes can be significantly reduced. A nonlinear conversion model was proposed to estimate the performance under low current densities from the results of the accelerated tests. The difference between the nonlinear model and the linear model can be 30% to 40%. When the current density is less than 2 mA/m^2, the service life regarding the anode–concrete interface can be longer than 70 years. For the critical chloride content, under a current density of 2 mA/m^2, the critical value can be increased nearly by a factor of two and the service life against chloride ingress can be increased by a factor of seven according to the DuraCrete model under the specific modeling condition.

Considering both the anode–concrete interface and the chloride content at the steel surface, it has been successfully proven that by applying low current densities, the service life of reinforced concrete structures can be significantly extended, to the range of 100 years or more. The cost of such ICCPre applications can be further reduced by using CFRP mesh anodes without compromising the performance of the system.

Keywords: Chloride initiated corrosion, cathodic protection and prevention, anode system, service life, durability, critical chloride content.

Sammanfattning

Katodiskt skydd med påtryckt ström (ICCP) och förebyggande (ICCPre) är tillförlitliga och effektiva tekniker för att stoppa, kontrollera och fördröja korrosion i armerade betongkonstruktioner. Den breda tillämpningen av denna teknik har dock begränsats av den höga kostnaden för anodsystemet. Dessutom är de långsiktiga elektrokemiska effekterna på anod–betong–gränssnittet och armeringsstålen fortfarande inte helt klara. Dessa effekter kan vara fördelaktiga eller ogynnsamma, vilket kommer att påverka strukturens prestationsförmåga och livslängd. Därför måste de långsiktiga elektrokemiska effekterna kvantifieras och beaktas vid dimensionering med avseende beständighet.

Denna avhandling har ägnats åt att få mer grundlig vetenskaplig förståelse i fråga genom experimentellt arbete. Ett nytt och kostnads effektivt kolfiberförstärkt polymer (CFRP)–nät användes som anodmaterial istället för traditionell metallanod. Accelererade test, med användning av relativt höga strömdensitet, användes för att utvärdera de långsiktiga elektrokemiska effekterna. Effekterna av de accelererade testen studerades och modellerades. Varierad karakteriserings- och övervakningsteknik användes för att analysera anod–betong–gränssnittet och stålets tillstånd samt kloridtröskelvärdet i betongen.

Resultaten visar att CFRP-näten är lämpliga som anodmaterial för katodiska förebyggande applikationer, med en livslängd på mer än 100 år. Kalkutlakning vid anod–betong–gränssnittet var oundvikligt som en följd av kemiska reaktioner och masstransporter under strömutbyte. De kemiska förändringarna kan orsaka materialförlust och öka betongens motstånd och så småningom få systemet att haverera. Med låg strömdensitet kan de kemiska förändringarna minskas betydligt. En icke-linjär omvandlingsmodell föreslogs för att uppskatta prestationsförmåga vid låg strömdensitet från resultaten av de accelererade testen. Skillnaden mellan den icke-linjära modellen och den linjära modellen kan vara 30% till 40%. När strömdensitet är mindre än 2 mA/m^2 kan livslängden för anod–betong–gränssnittet vara längre än 70 år. För kloridtröskelvärdet, under en strömdensiteten av 2 mA/m^2, kan det kritiska värdet ökas med nästan en faktor två och livslängden mot kloridinträngning kan ökas med en faktor sju enligt DuraCrete modellen under det specifika modeleringsförhållandet.

Med hänsyn tagen till både anod–betong–gränssnittet och kloridinnehållet på stålytan har det framgångsrikt visats att med användning av låg strömdensitet kan livslängden för armerade betongkonstruktioner ökas betydligt, upp till 100 år eller mer. Kostnaden för sådana ICCPre-applikationer kan minskas ytterligare genom att använda CFRP-nätanoder utan att äventyra systemets prestationsförmåga.

Nyckelord: Kloridinitierad korrosion, katodiskt skydd och förebyggande, anodsystem, livslängd, beständighet, kloridtröskelvärde.

Acknowledgments

Firstly, I would like to express my sincerest gratitude to my main supervisor, Prof. Luping Tang, for his trust and endless patience throughout my PhD journey. I can not think of anyone better as a supervisor than he is. He has shared his vast knowledge and experience, given valuable advices and insights, and provided a free and creative research environment for me. I have learned tremendously under his guidance, both scientifically and personally.

Besides my main supervisor, I would like to convey my appreciation to my co-supervisors, Associate Prof. Zareen Abbas, Dr. Urs Mueller, Dr. Jan-Erik Lindqvist, and Dr. Helén Jansson, for their knowledge and commitment at different stages of the project.

I am very grateful to Dr. Diana Bernin and Dr. Thomas Zack, for their assistance and constructive advices in NMR and LA-ICP-MS measurements. I would also like to thank our kind and lovely technician Marek Machowski, for his excellent support in the lab.

Finally, my sincere gratitude goes to all my colleagues, former and present, at the Division of Building Technology and the Division of Structural Engineering, for creating such a wonderful working environment and for your friendship. In particular, I thank my fellow PhD students at the research group of Building Materials, Arezou Babaahmadi (graduated in 2015) and Govindan Induchoodan, for all the great moments we shared together.

Last but not least, I want to direct my special thanks to my family, Brook and Victoria, for your absolute support through my PhD study. Your love and affection have been an indispensable source of power and inspiration for me, and none of this would have been possible without your unconditional love. I am also deeply grateful to my parents, who showed me the meaning of hard work and shaped me into an independent person.

Emma Qingnan Zhang

Gothenburg, April 2018

List of Publications

This thesis is based on the following appended papers:

Paper I. E. Q. Zhang, L. Tang, T. Zack. *Carbon fiber as anode material for cathodic prevention in cementitious materials.* Proceedings of 5th International Conference on Durability of Concrete Structures, Shenzhen, Guangdong, P. R. China, 2016, pp. 300–308.

Paper II. E. Q. Zhang, L. Tang, D. Bernin, H. Jansson. *Effect of the paste–anode interface under impressed current cathodic protection in concrete structures.* Materials and Corrosion (2018) 1–13. Available online.

Paper III. E. Q. Zhang, Z. Abbas, L. Tang. *Predicting service life of cathodic protection and prevention system in reinforced concrete using accelerated tests.* Submitted to Construction and Building Materials.

Paper IV. E. Q. Zhang, L. Tang. *Effect of cathodic prevention on chloride threshold content for as-received steel in concrete.* Submitted Electrochimica Acta.

List of Nomenclature

Acronyms

C/S	calcium to silica molar ratio
w/b	water to binder ratio
w/c	water to cement ratio
C-S-H	calcium silica hydrates
CH	calcium hydroxide or portlandite
ICCP	impressed current cathodic protection
ICCPre	impressed current cathodic prevention

Notations

σ_{L}	calcium leaching degree in cement paste	%
C_{cr}	critical chloride content in cement	wt% of cement
C_{dl}	doulbe layer capacitance	F
D	diffusion coefficient	cm^2/s
d_{L}	leaching depth in cement paste	mm
E	electric potential	V or mA
I	current	A or mA
i	current density	$\mathrm{A/m}^2$ or $\mathrm{mA/m}^2$
Q	electrical charge	C
q	electrical charge density	$\mathrm{C/m}^2$
R	resistance	Ω
t	time	s

Subscripts

a	apparent
an	anode
cat	cathode
$cell$	electrochemical cell
cor	corrosion
cr	critical
p	polarization
s	surface

Contents

Chapter 1

Introduction

1.1 Background

Corrosion of steel reinforcement is one of the major causes of damage or deterioration of concrete structures. Conventionally, to prevent reinforcement from corroding, a low water–cement (w/c) ratio is used in concrete to reduce the ingress rate of aggressive substances, and a large cover thickness is designed for prolonging the time needed by aggressive substances to reach the reinforcement steel during the specified service life. A large cover thickness simply implies a greater volume of concrete materials. Obviously, this conventional approach to the durability of concrete structures is at the cost of more CO_2 emissions and consumption of natural resources through consuming higher amounts of cement and constituent materials, which is against the fundamental ideas of sustainability.

The use of industrial by-products, such as fly ash and slag, as pozzolanic additions to partially replace Portland cement in the mixes is a usual approach to reduce the cement content in concrete. This approach is, however, strongly dependent on the availability of by-products with qualified pozzolanic properties. Due to stricter environmental regulations, coal power plants are reducing, implying less and less availability of fly ash in the future. With the technical development of the steel industry, the quality of slag may vary more and more.

Therefore, new and more sustainable approaches are needed for corrosion prevention and protection of reinforcement steel in concrete. Because concrete is porous and contains electrolytic pore solution, using the principle of electrochemistry in concrete is probably a more active way to prevent the reinforcement in concrete from corroding. In this way, the properties of concrete with a high w/c ratio may be better utilized.

1.2 Aim and scope

The aim of this work is to investigate the electrochemical aspects of impressed current cathodic protection (ICCP) and prevention (ICCPre) for reinforced concrete, regarding the durability and performance of ICCP systems as well as experimental and testing methods. To achieve this general aim, the following specific objectives have been defined:

- to characterize the anode–concrete interface under impressed current cathodic protection;
- to study the effect of accelerated testing of ICCP;
- to estimate the service life of an ICCP or ICCPre system based on accelerated test results;
- to investigate the effect of ICCP on the chloride threshold content of the reinforcement steel; and
- to evaluate the viability of using carbon fiber reinforced polymer (CFRP) mesh as anode material.

1.3 Scientific approach

An extensive literature study was conducted to analyze and compare the test methods and the experimental data available in the literature and thus identify the influence of the current density and choice of material from an electrochemistry and material science point of view.

In parallel, an experimental program was designed and carried out to investigate the research objectives. The experimental work basically included accelerated tests, which examine the chemical changes occurring at the anode–concrete interface and evaluate the effect of current density, and long-term monitoring tests which examine the influence of a preventative current density on the corrosion rate and the chloride threshold content of the reinforcement steel.

1.4 Limitations

Most of the limitations of this study are direct consequences of the choices and decisions made for the experimental work. Regarding the accelerated tests, it was focused on paste and mortar materials in favor of further microstructure analysis. In the case of long-term corrosion monitoring, parameters such as the w/c ratio and the cover thickness, which are well-known to play a fundamental role in corrosion

testing, were not considered variables. Moreover, only chloride-induced corrosion was investigated, hence the effect of carbonation was not taken into consideration.

The current densities and raw materials used in this work were chosen to be representative. In this case, for example in corrosion monitoring, only as-received steel bars were used, because the aim is to represent reality. Despite the large variety of carbon fibers available in the market, in terms of their different mechanical and electrical properties, aspect ratios, shapes, and dimensions, only one type of carbon fiber mesh was chosen to be tested as a demonstration.

However, the long-term corrosion monitoring is still on-going and further results regarding corrosion initiation and chloride threshold content are expected to be obtained in the future.

1.5 Outline of the thesis

This thesis consists of a report that summarizes this doctoral research project, as well as four appended papers.

Chapter 2 introduces the fundamental knowledge to establish the theoretical framework on which this work has been developed.

Chapter 3 describes the layout of the experimental work, in which the specifications of the materials and the design of the experiment set-up are presented.

Chapter 4 presents a detailed description of the analytical tools used for the material characterization, as well as the testing methods that were adopted or developed in this research.

Chapter 5 summarizes the main results and discussions from this project. More specific results are presented in the appended papers.

In Chapter 6, both general and specific conclusions from this study are drawn and suggestions for future research are given.

Chapter 2

Theoretical Framework

2.1 Corrosion initiation and pitting corrosion

In principle, the corrosion of metallic materials is an electrochemical process, which involves oxidation reactions at the anode and reduction reactions at the cathode. In the case of steel reinforcement corrosion, the reactions can be described in Equations 2.1.

$$Fe \rightarrow Fe^{2+} + 2e^{-} \tag{2.1a}$$

$$2H_2O + O_2 + 2e^{-} \rightarrow 4OH^{-} \tag{2.1b}$$

Figure 2.1 represents the passivation of steel in aqueous solutions, in terms of the potential–current density diagram. In the activity zone, the anodic current increases rapidly with the potential, because iron dissolves from the initial iron oxide. In the passive region, iron may continue to dissolve but at a very low rate and hence the corrosion rate is negligible. In the state of passivity, the steel is covered by a thin passivation layer (1–5 nm) composed of $\gamma-Fe_2O_3$ and Fe_3O_4 iron oxides (Küter 2009).

As shown in Figure 2.1, pitting corrosion occurs when the corrosion potential (E_{cor}) exceeds a critical value in the passive region of the polarization curve. This critical value is termed pitting corrosion (E_{pit}) and it decreases with the concentration of chloride ions (Bertolini et al. 2013).

Although it has been intensively studied for decades, the role of chloride ions in pitting corrosion is yet not fully understood. A breakdown of passivity is usually referred to three main mechanisms: the penetration mechanism, the film-breaking mechanism, and the adsorption mechanism (Strehblow and Marcus 2012). The penetration mechanism involves the transfer of aggressive anions, such as Cl^{-} and SO_4^{2-}, through the passive layer to the metal–oxide interface, where they cause further specific action (Hoar et al. 1965). The film-breaking mechanism requires discontinuities in the passive layer, such as cracks, that give direct access for the

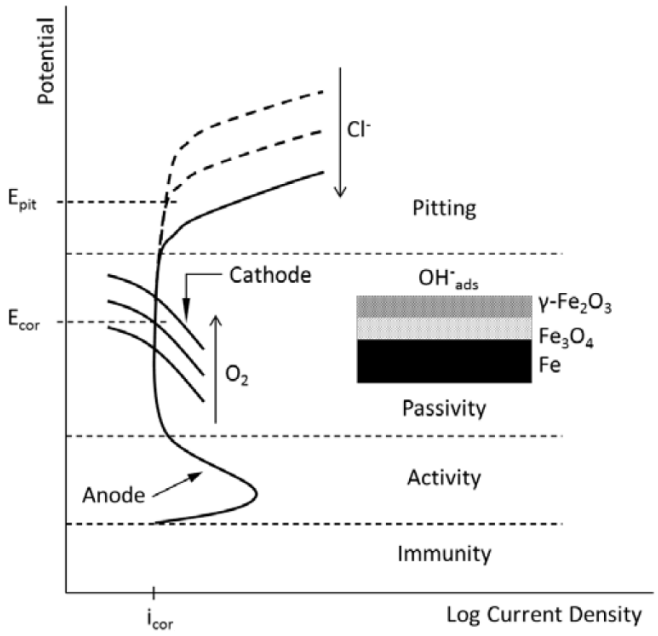

Figure 2.1: Polarization curve of steel (Silva 2013)

anions to the unprotected metal surface (Sato 1971). The adsorption mechanism proposes that the adsorption of aggressive anions at the passive layer surface leads to a progressive thinning of the passive layer until the start of an intense localized dissolution (Hoar and Jacob 1967). However, further investigation of the corrosion mechanisms is outside the scope of this thesis. Nonetheless, chloride ions, without doubt, play an influential role in the initiation of corrosion and the durability of reinforced concrete. Figure 2.2 illustrates the general electrochemical process of chloride induced pitting corrosion.

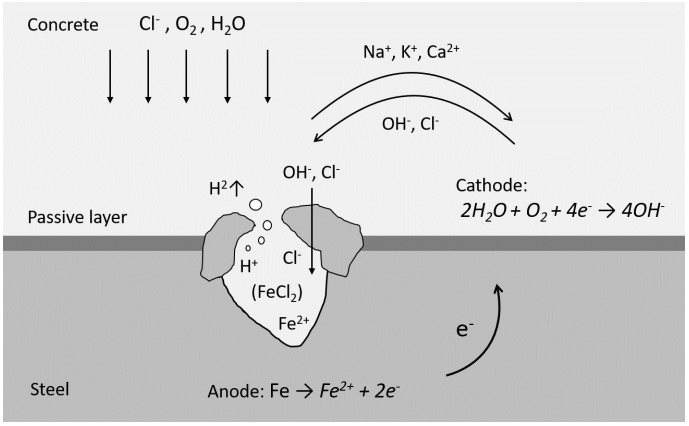

Figure 2.2: Schematic illustration of chloride induced pitting corrosion.

2.1.1 Critical chloride content

Studies of the initiation of chloride-induced corrosion of steel in concrete are often associated with the determination of critical chloride contents (C_{cr}), because of the

importance of this parameter in the service life design of reinforced concrete structures. There are two definitions of the chloride threshold content commonly used in the literature (Schießl and Raupach 1990; Angst et al. 2009):

- the chloride content at the steel surface that causes depassivation, from a scientific point of view; and
- the chloride content at the steel surface that leads to visible deterioration, from a practical engineering point of view.

Because the first definition has a fairly solid theoretical background, it has been adopted in this work, with certain reservations. Although the first definition is more precise than the second one, it has some ambiguity regarding the characterization of depassivation. As Andrade et al. (2003) points out, depassivation is not an instant nick point, but a period of time when depassivation and repassivation occur and it lasts until permanent "active corrosion" is established and progresses.

Despite a vast amount of research, the reported threshold values have a large scatter, because this value is affected by a number of factors, such as the pH of the pore solution, the steel potential, binder type, w/c ratio, surface condition of the steel, steel–concrete interface, moisture and oxygen content, temperature, source and accompanying cations of chloride ions, inhibitors, and electrochemical treatment (Angst et al. 2009).

2.1.2 Chloride content measurement

The measurement of the chloride content in cementitious materials is of great importance because of its significant influence on the evaluation of the chloride threshold content in concrete and durability-related design. The determination of the chloride content in cementitious materials is well-documented in standards (*AASHTO T 260-97* and *ASTM C1152/C1152M*) and technical reports (Andrade 2002).

The measurement procedure usually involves the extraction of chloride from powder samples, followed by quantification using titration techniques. Nonetheless, a number of different extraction and quantification methods have been proposed (Chaussadent and Arliguie 1999; Climent et al. 1999). For instant, X-ray fluorescence spectrometry (XRF) has been used to measure the total chloride content, which can significantly reduce sample preparation and time for analysis (Dhir et al. 1990; Proverbio and Carassiti 1997). Innovative approaches, such as high spatial resolution scanning techniques, have also been investigated to further improve the measurement precision, reduce sample preparation time, and other advantages. Laser ablation inductively coupled plasma mass spectrometry (LA-ICP-MS) has been used to analyze the chloride distribution along the concrete–steel interface, by which it enables continuing profiling of multiple elements and direct analysis on the sample surface (Silva 2013).

2.1.3 Corrosion monitoring

There are many non-destructive techniques available for measuring and monitoring the corrosion rate of steel reinforcement in concrete structures, for example using electrochemical principles (Ahmad 2003). Reinforcement corrosion can be assessed by electrochemical methods, such as open circuit potential (OCP) measurement, resistivity measurement, polarization resistance measurement, galvanostatic pulse method and electrochemical impedance spectroscopy (EIS). In this research, two methods have been adopted. Their working principles and criteria will be presented here briefly.

Open circuit potential measurement

The open circuit potential (OCP) measurement is also commonly referred to as half-cell potential measurement. The interpretation of OCP criterion is given in Table 2.1, where CSE represents the copper–copper(II) sulfate electrode and SCE stands for saturated calomel electrode.

Table 2.1: Interpretation of half-cell potential values as per *ASTM C876-15*

Half-cell potential (mV CSE)	Half-cell potential (mV SCE)	Corrosion level
> -200	> -127	Low (10% risk of corrosion)
-200 to -350	-127 to -277	Intermediate risk corrosion
< -350	< -277	High (90% risk of corrosion)
< -500	< -426	Severe corrosion

Although OCP measurement is probably the most commonly used method for corrosion detection, it can be easily influenced by many factors, such as oxygen availability and moisture. If the judgment was made solely based on this criterion, it may lead to a large risk of error and a high probability of improper interpretation. Hence, the OCP criterion was used as a supplementary indicator in this research.

Galvanostatic pulse method

The galvanostatic pulse method can be used to assess the corrosion current density of steel reinforcement in concrete (Tang and Fu 2006). This method is a transient polarization technique working in the time domain. A constant anodic or cathodic current is imposed on the reinforcement for a short time and the reinforcement is polarized in the anodic or cathodic direction compared to its free potential. The change of the electrochemical potential is then recorded against a reference electrode

by data acquisition systems as a function of the polarization time. A typical potential response is shown in Figure 2.3.

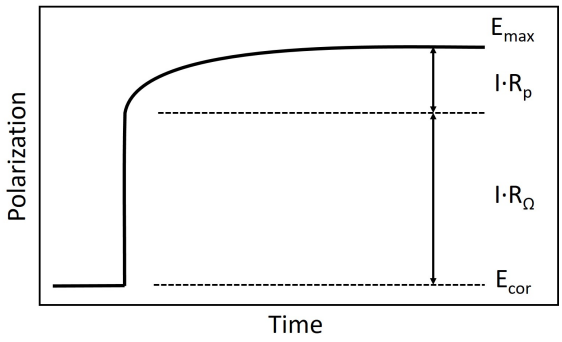

Figure 2.3: A typical potential–time curve as response to a galvanostatic pulse.

Table 2.2 lists commonly quoted general corrosion currents and their basic interpretation (Davies and Broomfield 2013). The corrosion current is expressed in μA/cm^2 throughout this thesis. Because the corrosion rate is a quantitative measurement of the degree of corrosion of steel, it was used as a main indicator in this research.

Table 2.2: Corrosion currents —Steel in concrete (Davies and Broomfield 2013)

Corrosion rate (μA/cm^2)	Corrosion rate (mA/m^2)	Corrosion level
< 0.1	< 1.0	Passive —very low corrosion
0.1–0.5	1.0–5.0	Low to moderate corrosion
0.5–1.0	5.0–10.0	Moderate to high corrosion
> 1.0	> 10.0	High corrosion
1.0–10.0	10–100	Very high corrosion

2.2 Cathodic protection and prevention

2.2.1 Definition and principles

Cathodic protection and prevention is now well accepted as a powerful and efficient method for reducing corrosion rate and improving corrosion resistance of reinforcing steel in concrete (Bertolini et al. 1998). Impressed current cathodic protection (ICCP) is achieved by means of an anode system usually laid on the concrete surface and connected to the positive terminal of a direct voltage source, while the reinforcement acts as a cathode and is connected to the negative terminal.

By shifting the electrical potential negatively, the reinforcements are forced into a passivity or immunity state. In some cases, cathodic protection is called *cathodic prevention* when it is applied to new structures that are expected to become contaminated by chloride during their service life. A small cathodic polarization of the steel should be applied at the beginning of the service life. The current density for cathodic protection is 2–20 mA/m^2 (of steel surface) and for prevention it is 0.2–2 mA/m^2, according to *BS EN ISO 12696*.

Figure 2.4 illustrates the principle of cathodic protection and prevention. Cathodic prevention is applied from the beginning at point 1 and to points 2 and 3, so that the potential is maintained in zone B (1→2→3); cathodic protection is applied only after corrosion has initiated at point 4, for restoring passivity, the potential shift should be in zone B (1→4→6) and for reducing the corrosion rate, the potential should be shifted into zone C (1→4→5).

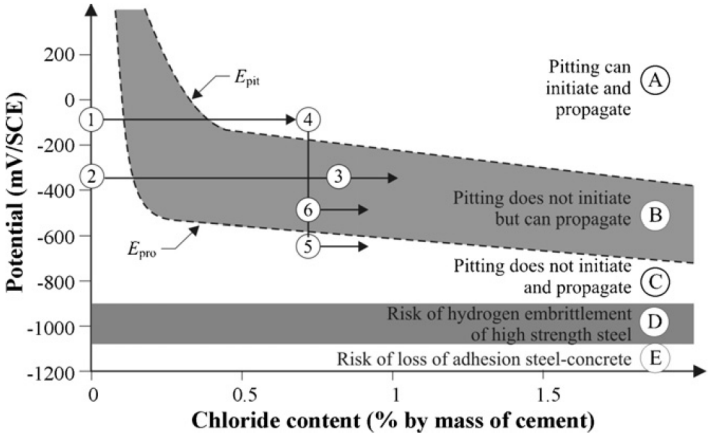

Figure 2.4: Schematic illustration of the working principles of ICCP and ICCPre (Bertolini et al. 2009).

2.2.2 Electrochemical aspects

In an electrochemical cell, such as an ICCP system, chemical reactions occur at both the anode and the cathode, and ions are current carriers that are transported through the concrete, which can be summarized as a coupled process of chemical reaction and mass transport.

At the cathode, hydroxide ions are produced as

$$2H_2O + O_2 + 4e^- \longrightarrow 4OH^- \tag{2.2}$$

which is beneficial for maintaining an alkaline environment around the steel reinforcement.

At the anode surface, the chemical reaction occurring is mainly the oxidation of hydroxide ions (OH^-) as

$$4OH^- \longrightarrow 2H_2O + O_2 + 4e^- \tag{2.3}$$

As this reaction progresses and the anode–concrete interface loses its basic character, oxidation of water takes place to produce hydrogen ions (H^+) (Cramer et al. 1999):

$$2H_2O \longrightarrow O_2 + 4H^+ + 4e^- \tag{2.4}$$

Both reactions consume hydroxide ions and tend to lower the pH at the anode–concrete interface, which can be considered as acid formation at the anode.

Chlorine gas is produced when chloride is present, as shown in Reaction 2.5a. At a pH of 8 or lower, an equilibrium of chloride acid and hypochlorous acid is also present, as given in Reaction 2.5b (Zebger et al. 2005).

$$2Cl^- \longrightarrow Cl_2 + 2e^- \tag{2.5a}$$

$$Cl_2 + H_2O \rightleftharpoons HCl + HClO \tag{2.5b}$$

The type of anode reaction depends on the electrical potential, the availability of reactants, and the type of anode material. The reaction rate mainly depends on the current density and the availability of ions.

Under an electric field, positive ions (Na^+, K^+ and Ca^{2+}) in the concrete pore solution migrate towards the reinforcement steel, and negative ions (OH^-, Cl^- if available) migrate towards the anode. The migration flux of the ions depends on the concentration of the ions, which can be calculated from the applied current density and transference number. The transference number is defined as the fraction of a current carried by a certain type of ion (Newman and Thomas-Alyea 2012).

Concrete, not only as a transport medium, also actively reacts with the process. Concrete is porous and highly alkaline, so when the pH is decreased, cement hydrates dissolves and releases hydroxide ions, which is associated with calcium leaching and degradation of the cement paste.

From a thermodynamic point of view, if the concentration of calcium ions decreases, calcium hydroxide crystals (CH or portlandite) dissolve to replenish the calcium ions to maintain equilibrium. After complete dissolution of CH, calcium ions are supplemented by the calcium silicate hydrates (C-S-H) and the C-S-H finally degrades to silica (SiO_2) gel (Brown and Clifton 1988). The equilibrium between CH and C-S-H and their component ions in the pore solution is described by the following reactions (Saito and Deguchi 2000):

$$Ca(OH)_2 \rightleftharpoons Ca^{2+} + 2OH^- \tag{2.6}$$

$$C\text{-}S\text{-}H \rightarrow Ca^{2+} + 2OH^- + SiO_2 \tag{2.7}$$

2.2.3 Criteria of ICCP

BS EN ISO 12696 specifies the criteria applied to cathodic protection of steel in concrete, with the concrete atmospherically exposed, buried or immersed. The criteria are:

> *For any structure, any representative steel in concrete location shall meet any one of the three criteria given in terms (a) to (c):*
>
> *(a) an "Instantaneous OFF" potential more negative than -720 mV with respect to Ag/AgCl/0.5 M KCl; or*
>
> *(b) a potential decay over a maximum of 24 h of at least 100 mV from "Instantaneous OFF"; or*
>
> *(c) a potential decay over an extended period (typically 24 h or longer) of at least 150 mV from the instant off subject to a continuing decay and the use of reference electrodes (not potential decay probes) for the measurement extended beyond 24 h.*

If the instantaneous off potential is more negative than -720 mV, the steel meets criterion (a). If this does not occur, the measurement of potential change over time is used to assess the performance of the system. In the case of criterion (b), the curve of potential change is typically considered to be exponential. Criterion (c) is included to address cases, such as in low oxygen environments, where a greater decay is required over a longer period. These standard criteria usually can ensure sufficient protection applied to the structure. However, in some special cases, such as in a marine environment, these conventional criteria may not be reliable. Moreover, as more knowledge has been gained about ICCP systems over the past three decades, more appropriate criteria, adapted to different exposure conditions, have had to be further investigated and and are needed for engineering use in field applications.

It has been argued that criterion (a) may not be the most appropriate criterion, because it changes the local environment and the steel surface conditions when imposing a cathodic current, such as the removal of aggressive ions and the production of hydroxyl ions (Glass and Chadwick 1994). Instead of achieving an absolute negative potential shift, the use of potential depolarization and current density related criteria are more appropriate in cases where the purpose of cathodic protection is to induce or restore passivity (Glass and Chadwick 1994).

In some experimental work, the interruption time for measuring depolarization was chosen to be 4 h instead of 24 h, so as to achieve 100 mV decay (Bertolini et al. 2004; Bertolini et al. 2009). There are also suggestions for the use of different decay values instead of the conventional 100 mV in criterion (b). Henriksen (1980) proposed a value of 50 mV for engineering practice, although he found that 30 mV also can provide protection. New assessment methods have also been tested and proposed, with a low risk of predicting false positives, without imposing any requirement of collecting an instant off potential, and enjoying a data logging time between 5 and 30 min, to be used to estimate whether 100 mV decay would be achieved (Atkins et al. 2017).

Bahekar and Gadve (2017) has reported that 5 mA/m^2 is the most appropriate protection current density for reinforced concrete. Glass et al. (2000) suggested that an initial integrated protection current density of 6 mA/m^2 or more may be

required, whereas lower current densities may be applied once lower corrosion rates have been induced.

Besides depolarization potential and current density related criteria, a time-dependent potential shift criterion has also been studied. Based on the idea of persistent protection attributed by Hoar in 1967, intermittent CP was studied by Glass et al. (2001), which can be utilized in the tidal zone environment and provide a justification of a current density criterion for a relatively dry or wet condition.

Although evaluating and developing protection criteria has not been the research focus in this thesis, it is of great importance in the applications in engineering practice and definitely deserves further research effort. In the research work presented in this thesis, a depolarization decay criterion was adopted for the evaluation of the protection efficiency. It was presented and discussed in Paper IV.

2.3 Effects of ICCP

The beneficial effects of long-term cathodic protection can be summarized by three points (Pedeferri 1996): (1) the corrosion rate is reduced or can even be negligible by taking the steel into the passivity or immunity state; (2) increased alkalinity enables the steel to restore passivity because of the production of hydroxide ions at the steel surface; (3) the concentration of chloride ions is decreased because of the migration of chloride ions away from the steel reinforcement (Eichler et al. 2010).

Nevertheless, due to the application of an electric current, there is a potential risk of degradation or early deterioration of the system, which would influence the overall performance and the service life of the ICCP system. The reasons for CP system failure vary from case to case. However, they can be summarized as: power unit failure, anode–copper connection error, reference electrode failure, and degradation of anode materials (Polder et al. 2014). The failures of different components have different effects, for example, some occur instantly, such as a central power unit failure, whereas another may not be apparent in an inspection survey, such as anode degradation.

Anode degradation is caused by the formation of acid in the bond plane or the oxidation of the anode material itself. It will lead to an increase in the cell's resistance and a loss of adhesion between the anode and concrete (Mietz et al. 2001). However, the mechanisms of anode–concrete interface durability in an ICCP system are still not fully understood, that is, whether it is the loss of adhesion due to calcium leaching or low pH environment hindering the electrochemical functioning (Peelen et al. 2008). The mechanism of acid formation will be briefly presented here in Section 2.3.1, as it was one of the main research focuses in this work.

2.3.1 Acidification at the anode

Due to the nature of electrochemical reactions, ICCP transforms the microstructure of the concrete around the steel over a period of time due to the migration of the ionic species and the chemical reactions (Pedeferri 1996; Eichler et al. 2010). One of the major reasons for a system failure is the degradation at the anode–concrete interface due to acid formation in the bond plane, which is associated with calcium leaching (Polder and Peelen 2011; Mietz et al. 2001; Polder et al. 2002; Polder et al. 2014). The CP-related acid formation can lead to early failure or unplanned maintenance for ICCP systems (Polder et al. 2014).

Figure 2.5 illustrates schematically the possible migration and diffusion processes (adopted from Bertolini et al. (2004)). To calculate the acid formation at the anode surface, the amount of acid produced (or hydroxide consumed) can be determined from the total charge passage. Theoretically, one mol of electron produces one mol of acid at the anode, which is equal to one mol of calcium dissolution. However, studies have found that the observed amount of dissolution was less than what was expected from oxidation and migration, suggesting that diffusion has compensated part of the acid formation (Polder et al. 2002; Polder and Peelen 2011).

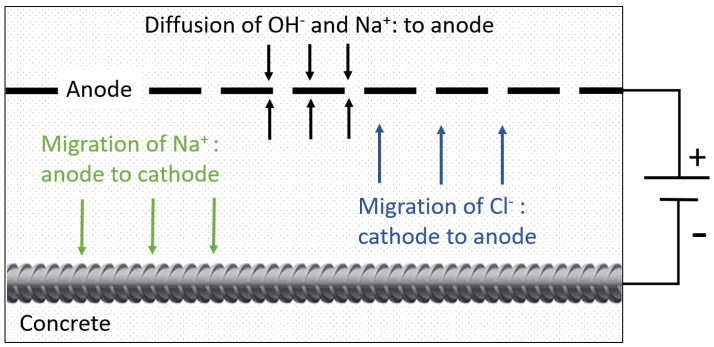

Figure 2.5: Schematic illustration of electrode reactions, migration and diffusion of ions (adopted from Bertolini et al. (2004))

A brief discussion of the migration and diffusion process is presented in the following. The overall effect of migration for an ICCP system is that hydroxide and sodium ions become depleted at the anode and accumulated at the cathode. When a concentration gradient has built up, it will cause these ions to diffuse from elsewhere in the concrete towards the anode, and from the cathode to elsewhere (Polder and Peelen 2011). This means that, for normal ICCP current densities (below 20 mA/m^2), the diffusion flux has the same order of magnitude as the migration flux, so that the consumption rate of hydroxide ions at the anode is relatively low and calcium leaching is also slow (Polder and Peelen 2011).

However, for significantly higher current densities, such as in accelerated tests, the contribution of diffusion is smaller, and the pH reduction as well as the anode–concrete interface degradation caused by calcium leaching is greater. This effect has been considered in this thesis when converting accelerated test results to normal test conditions.

Qualitative numerical models have been proposed to describe concrete acidification and the transport of calcium hydroxide under cathodic protection (Peelen et al. 2008; Koster et al. 2010). Interesting results from Peelen et al.'s model (2008) showed that sodium ions do not affect the acidification rate of concrete: it was merely a re-distribution process as it did not involve any chemical reactions, which is contradictory to the common understanding that sodium ions should accumulate at the cathode.

Because the electrochemical processes of ICCP in concrete are very complex and involve several transport mechanisms and chemical reactions, it is quite a challenge to take all the possible aspects into consideration in one model. Some of the effects of chemical reactions on ionic transport in concrete have been reviewed by Samson et al. (2000). Some parameters, such as the dissolution rate of $Ca(OH)_2$ from cement paste, were unknown and have to be assumed for modeling purposes (Peelen et al. 2008). Prediction of the dissolution behavior of $Ca(OH)_2$ is needed to be further validated experimentally in order to be used with confidence (Koster et al. 2010).

Although numerical models can shed some light on the concrete degradation caused by calcium leaching or acidification, there are still many unsolved questions that need to be investigated experimentally. Hence, one of the main objectives of this work has been to examine the effects of ICCP regarding service life and anode–concrete durability, to bring some new aspects to this issue.

2.3.2 Critical chloride content under ICCP

It has been proven both experimentally and numerically that small preventative cathodic currents can not stop chloride ingress into the concrete (Bertolini et al. 2009; Tang et al. 2012). However, according to Bertolini et al. (2009), a small cathodic current can increase the chloride threshold value for the initiation of corrosion by reducing or eliminating the potential difference on the steel surface and, therefore, maintaining the reinforcement in passivity even in the presence of very high contents of chlorides.

By applying a low current density, a small amount of cathodic polarization is induced in the reinforcement, which is able to keep the steel potential below the pitting potential, so that passivity can be retained even in chloride-contaminated concrete. Moreover, hydroxide ions are produced at the steel surface according to the cathodic reaction. The production of alkalinity will benefit maintaining the pH level near the steel surface (Polder et al. 2011). Because the breakdown of the passive layer also depends on the presence of other inhibitors, such as OH^-, as suggested by $[Cl^-]/[OH^-]$, the protective effects associated the production of hydroxide ions may be more important than those related to the removal of chlorides in the case of ICCPre.

Bertolini et al. (2009) have reported that by applying very small current densities, 0.4 and 0.8 mA/m^2, to the steel surface, the chloride content close to the steel

reinforcement was 1.5 wt% of cement mass, higher than that in the control specimen in the absence of cathodic prevention, in which the chloride content was 0.7 wt% of cement mass. However, it is worth noting that the chloride content obtained from the control specimen was that when the corrosion was observed on 2.5% of the total steel surface, which may have led to a higher value of chloride content than that of the depassivation definition, as discussed in Section 2.1.1.

There is still very little reported data on how cathodic prevention influences the chloride threshold content, given the well-known problem of the large scatter in the data on chloride threshold content measurement in general. More documented data in both laboratory tests and field application is greatly needed in order to understand the mechanism and evaluate the effect of small cathodic currents on the initiation of corrosion. Moreover, similar to the case for chloride threshold content measurement, there is a need for proper testing methods that can provide good reproducibility and repeatability. Therefore, this thesis work was partly aimed at contributing some knowledge and effort to this field.

2.4 Development and challenges of anode systems

The anode system, as a key component in a cathodic protection or prevention system, has a great impact on the performance and durability of the system. Mixed-metal oxide titanium (MMO/Ti) anodes have gained great acceptance for CP applications because of their high current capacity, light weight, and low consumption rate (Heidersbach et al. 2006). However, their extensive use has been prevented by their high cost (Dreyman 1972). Polymer composite anodes, especially carbon fiber composites, as an attractive alternative, have nowadays shown great potential due to their affordability, good electrical properties, and versatility in manufacture.

Carbon based material, being considered the material of future technology, has drawn great attention and been under extensive study. Kessler and Powers (1989) have developed a type of conductive rubber anode for steel reinforced concrete structures in a marine environment, which contains ethylene-pylene-diene monomer (EPDM) and conductive carbon black. Graphite conductor embedded polymer anodes have been used for cathodic prevention in coastal reinforced concrete structures (Heidersbach et al. 2006). A conductive coating overlay containing graphite or carbon fiber reinforced cement has been verified to be suitable for use in a cathodic protection system (Jing and Wu 2011; Bertolini et al. 2004; Darowicki et al. 2003).

However, investigations of carbon fiber composites as anodes for CP/CPre system are relatively new (Mahdi 2010; Mayer 2004). Mork et al. (2006) found that carbon fiber mesh anode showed no loss of weight and no defects when the system was applied to polarization voltages up to 1.8 V and the protection current 1–2 mA/m^2. Mahdi (2010) reported in his doctoral thesis that carbon fiber composite can be

used as the anode material in cathodic protection and prevention systems but the polarization potential should not be above 300 mV, although this value was much lower than that Mork et al. (2006) has reported. The functioning life of the system might be estimated based on the weight loss of the carbon-based anode (Polder and Peelen 2011). In a technical report, Mork et al. (2007) also monitored and investigated a harbor structure in Honningsvaag in Norway. The anode system consisted of carbon fiber meshes and cement based mortar and the CP system was achieved by a current density of 2 to 5 mA/m^2 and a voltage of a maximum of 1.8 V. The system was functioning well as of the day of publishing, according to *BS EN ISO 12696*.

Attempts have been made to combine the reinforcing property together with the anode function, which have demonstrated the successful application of CFRP as dual-functional material for ICCP in laboratory (Lambert et al. 2015; Zhu et al. 2016b; Tang et al. 2012). A CFRP anode can operate at 128 mA/m^2 with a relatively low consumption rate (Nguyen et al. 2012b), and the ultimate strength of the concrete increases by approximately 13.5% using a surface-mounted CFRP fabric (Nguyen et al. 2012a). The degradation mechanism of a CFRP anode has been investigated in simulated solutions and a concrete environment (Sun et al. 2016a; Sun et al. 2016b; Zhu et al. 2015). Based on their results, Zhu et al. (2016a) and Sun et al. (2015) suggest that the polymer matrix is sensitive to electrochemical degradation but the carbon fiber remains with very little loss of mass even at very high current densities (up to 3 A/m^2 of anode surface).

Despite the many attractive properties of the CFRP material, its application as an anode for an ICCP or ICCPre system is still rare and limited. One goal of this PhD work, therefore, is to provide more scientific evidence on the viability of using CFRP as an alternative anode material for ICCP or ICCPre applications in reinforced concrete structures.

2.5 Durability design and service life aspects

2.5.1 Concrete cover

The *DuraCrete* model is probably the most commonly used guideline for durability design and redesign (Engelund et al. 2000). The design equation for chloride initiated corrosion is

$$g = C_{cr}^{d} - C^{d}(x,t) = C_{cr}^{d} - C_{s,cl}^{d}\left[1 - erf\left(\frac{x^{d}}{2\sqrt{D_{cl}^{d}(t)\cdot t}}\right)\right] \tag{2.8}$$

where C_{cr}^{d} is the design value of the critical chloride content; $C_{s,cl}^{d}$, the design value of the chloride surface content; x^{d}, the design value of the cover thickness; D_{cl}^{d}, the design value of the diffusion coefficient of chloride ingress; and t is the time.

The design value of the cover thickness (x^d) can be determined when all the parameters are given. The characteristic value of the cover thickness (x^c) is found from

$$x^c = x^d + \Delta x \tag{2.9}$$

where Δx is the safety margin for the cover thickness and x^c is used in drawings and for reinforcement detailing.

The design value of the time dependent resistance is derived from

$$D_{cl}^d(t) = k_{e,cl} \cdot k_{c,cl} \cdot D_{cl} \cdot \left(\frac{t_0}{t}\right)^{n_{cl}} \cdot \gamma_{D_{cl}} \tag{2.10}$$

where $k_{c,cl}$ is the curing factor; $k_{e,cl}$ is an environmental factor; t_0 is the age of the concrete when the compliance test is performed; n_{cl} is the age factor; $\gamma_{D_{cl}}$ is a partial factor for the diffusion coefficient with respect to chloride ingress, here it is taken as $\gamma_{D_{cl}} = 1$; and D_{cl} is the diffusion coefficient with respect to chloride ingress determined on the basis of the Rapid Chloride Migration (RCM) test according to *NT Build 492*, which can be also written as D_{RCM}.

A typical value for C_{cr}^d is 0.4% by mass of binder for the environment with sufficient oxygen, such as an atmospherically exposed condition. For an environment with limited oxygen, C_{cr} is higher. Tang and Utgenannt (2009) has reported the threshold value was 1% by mass of binder in a field study where the concrete slabs were half submerged in seawater and half exposed to air.

As an example, for OPC concrete with a w/c ratio of 0.4, the chloride diffusion coefficient, D_{RCM}, is 12.2×10^{-12} m^2/s tested by the RCM test according to *NT Build 492* (Tang 2008). In the case of submerged concrete structures, if C_{cr} was chosen to be 1% by mass of binder, the designed values of the cover depth would be 40 mm for a service life of 25 years and 50 mm for a service life of 50 years, as shown in Figure 2.6. Taking the safety margin as 14 mm, the characteristic values of cover depth are then 45 mm for a service life of 25 years and 65 mm for a service life of 50 years.

Eurocode 2 also identifies the minimum value of the cover thickness. The minimum cover thickness for durability, $c_{min,dur}$, depends on the exposure classes of the environment and the structural class of the steel reinforcement. *Eurocode 2* defines the sequence for determining the concrete cover. The nominal value, c_{nom}, which should be stated on the drawings, is calculated by

$$c_{nom} = max[(c_{min} + \Delta c_{dev}); 20 \text{ mm}] \tag{2.11}$$

where c_{min} has considered both for the durability and the bond. The value of c_{dev} for buildings and bridges may be defined in the National Annex and is recommended by *Eurocode 2* to be taken as 10 mm.

For earth retaining walls and foundations, $c_{nom} = 40$ mm is common, due to the difficulty of visual inspection to detect deterioration. An example was given in "Designers' Guide to EN 1992-2 Eurocode 2": to determine a C40/50 deck slab with

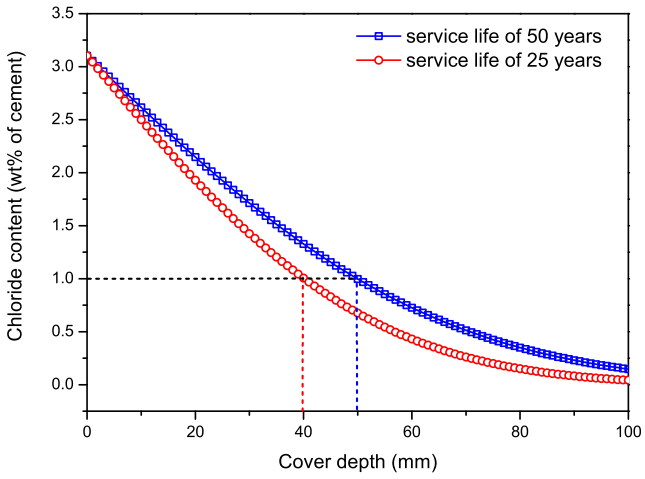

Figure 2.6: An example of DuraCrete model

a service life of 100 years, given the parameters with exposure class XC3 and structural class S4, the nominal concrete cover c_{nom} is 35 mm.

2.5.2 Service life of ICCP systems

An ICCP system includes many components that can influence the service life as a whole, such as the main power unit, rectifier, and reference electrodes. Among these components, the anode system is the most expensive and important component in terms of both cost and performance. The anode system consists mainly of three elements: the anode material itself (MMO-Ti or CFRP), which in turn is fed by primary anodes (a metal strip or wire) and linked through an anode–cable connection to the power unit. The anode system may account for 60% to 90% of the total cost, depending on the size of the system (Polder et al. 2014).

To assess the service life of an ICCP system is also a complicated issue, depending on the failure modes of the different components, the impact on the system varies. For example, a power unit failure due to a lightning strike will cause the whole system to shut down and can be immediately noticed and repaired. A malfunctioning reference electrode will give an abnormal recording and may not be easy to detect. Anode degradation, which is the main focus of this thesis, can cause an increase in the resistance and a loss of adhesion. This will in turn cause the driving voltage to increase, further accelerating degradation. Eventually it became impossible to maintain sufficient current for full protection to the steel reinforcement (Mietz et al. 2001). The service life of the anode system may be determined mainly by acid production due to current exchange (Ali et al. 1992). When a global anode failure has happened, it needs complete replacement for the anode system, involving a high cost.

Therefore, it is crucial to minimize the acid production by controlling the current

density and estimating the degradation for a better service life design.

Chapter 3

Experiments

3.1 Raw materials

Ordinary Portland cement (OPC) and supplementary cementitous materials (SCMs) were used as the raw materials for the concrete mixture. An innovative material, carbon fiber reinforced polymer (CFPR) mesh, was used as the anode material. Normal carbon steel was used as the reinforcement.

3.1.1 Portland cement and SCMs

Swedish structural cement CEM I 42.5N-SR3 MH/LA was used in this work as ordinary Portland cement (OPC). Two types of supplementary cementitious materials were also included: an ASTM class F siliceous fly ash (FA), manufactured by Noecem AS (Norway), and ground-granulated blast-furnace slag (GGBS), commercially available as Merit 5000, supplied by Merox (Sweden). The chemical compositions of the OPC, FA and GGBS are given in Table 3.1.

3.1.2 CFRP anode

The CFRP mesh anode used in this research was manufactured by the SGL Group and is commercially available as SIGRATEX Grid. Figure 3.1 shows the shape and dimensions of the mesh. The spacing of the mesh was about 25 mm by 25 mm. The dimensions of the cross-section of the CFRP bundle were 3 mm in width in the vertical direction and 2 mm in the horizontal direction. The thickness of the mesh was approximately 0.6 mm. The circumference of a fiber bundle in the vertical direction was 15 mm. The type of polymer coating was unknown. The mass percentage of polymer was 15%, measured by thermogravimetric analysis (TGA) by the author. The measured resistivity per unit length was about 0.05 Ω.

Table 3.1: Chemical compositions (wt%) of OPC, FA and GGBS

Composition	OPC	FA	GGBS
CaO	64.5	5.1	31
SiO_2	22.5	54.7	34
Al_2O_3	3.1	21.7	13
MgO	1.3	2.1	17
SO_3	2.6	0.9	0.25
TiO_2	–	0.9	2.4
Fe_2O_3	4	8	–
Na_2O	0.12	0.9	–
K_2O	0.58	2.1	–
Cl	0.01	0.01	–
Na_2O_{eqv}	0.5	2.3	0.09
FeO	–	–	0.4
S^{-2}	–	–	1.3
P_2O_5	–	0.7	–
Cr_2O_3	–	0.01	–
Mn_2O_3	–	0.1	–
SrO	–	0.2	–
ZnO	–	0.02	–
Carbon (C)	–	1.9	–

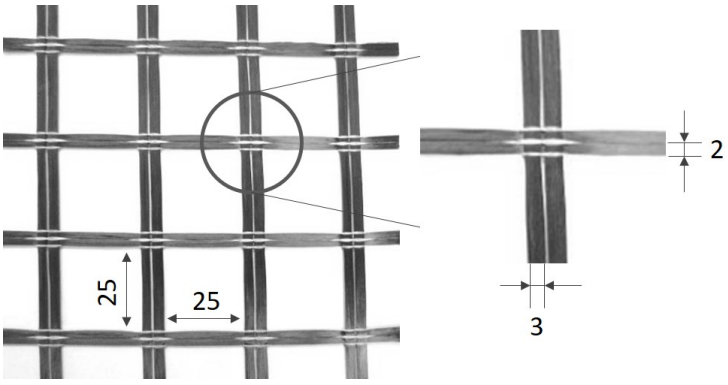

Figure 3.1: CFRP meshes as anode material. All values are in mm.

3.2 Test specimens

Three types of specimens were included in this work: paste, mortar, and concrete. The Paste specimens were mainly used for the anode–paste interface analysis after the accelerated tests, and partly for service life modeling. The mortar specimens were used for the service life modeling. The concrete specimens were tested for the corrosion monitoring and the chloride threshold analysis.

Table 3.2 summarizes the mix proportions of all specimens in overview. The first letter in the category represents the type of the specimen and the second letter indicates the type of binder; P stands for ordinary Portland cement, F for fly ash, and G for GGBS. The largest size of aggregate for the concrete was 12 mm. Detailed descriptions are given below in separate sections.

Table 3.2: Mix proportions of test specimens

	Paste	Mortar			Concrete
Category	P	M-P	M-F	M-G	C-P
Water to binder (w/b) ratio	0.4	0.6	0.6	0.6	0.4
Binder effectivity factor	1	1	0.4	0.6	1
Cement content (kg/m^3)	1400	500	460	430	436
Water content (kg/m^3)	560	300	300	300	174
Sand content (0-4 mm) (kg/m^3)	1500	1500	1500	1500	–
Aggregate content (kg/m^3)	–	–	–	–	1843
Fly ash content (kg/m^3)	–	–	90	–	–
Slag content (kg/m^3)	–	–	–	110	–
Reactive CaO% of SCMs	–	–	5%	31%	–
equivalent CaO content (kg/m^3)	900	–	296	309	–
Slump (mm)	–	–	–	–	35
σ_{cube}^{28d} (MPa)	–	–	–	–	97

3.2.1 Paste specimen

The paste specimens were subjected to accelerated tests and grouped as P-i6 and P-i3, where '6' and '3' indicate the current applied, in mA. The dimensions of a specimen are illustrated in Figure 3.2. Each specimen contained a single Φ10 mm plain steel bar as cathode and two bundles of CFRP as anode. The effective anode surface area was 16 mm^2. All surfaces were coated by epoxy resin to prevent

unwanted penetration of chloride, except the curved surface in front of the CFRP anode for one-dimensional chloride penetration. The position of the uncoated surface is shown in Figure 3.2 as well. The bottom of the steel bars and the CFRP anode were wrapped with insulation tape. The specimens were partially immersed in a 3% NaCl solution during the test.

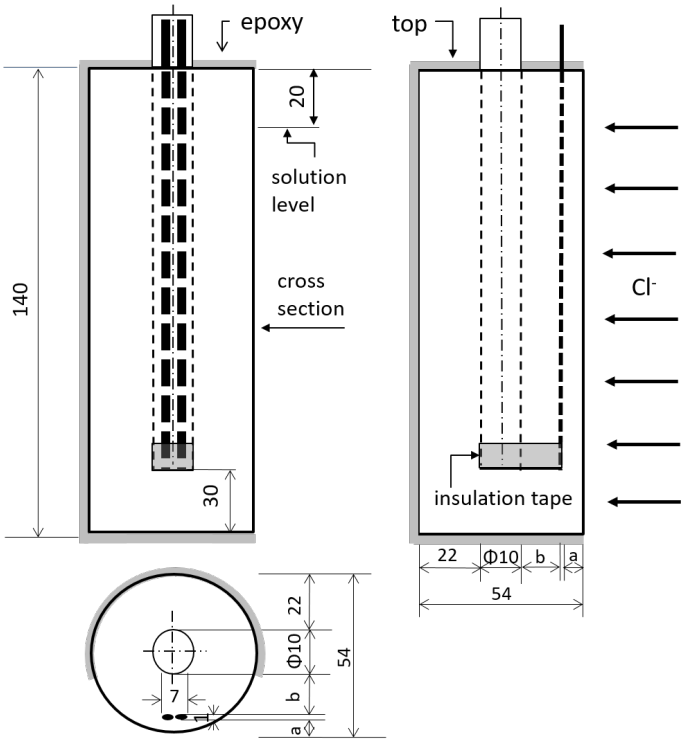

Figure 3.2: The 3-view drawing of a paste specimen. Chloride penetration direction is indicated by arrows. $a = 7 \sim 10$ and $b = 10 \sim 15$. All values are in mm.

3.2.2 Mortar specimen

For the mortar specimens, the cement content was replace either by 20% (by weight) of fly ash or by 25% (by weight) of slag, which are denoted by the group names M-F and M-G. The content of reactive calcium oxide (CaO) in the fly ash used in the tests was 5%, but 31% for the slag.

Figure 3.3 illustrates the dimensions of the specimens and the location of the anode. Each specimen contained two Φ10 mm plain steel bars as cathode and CFRP anode mesh as anode. The effective area of the anode surface in a mortar specimen was 400 cm^2. All surfaces were coated by epoxy resin to prevent unwanted penetration of chloride, except the exposure surfaces in front of the CFRP anodes for one-dimensional chloride ingress. The mortar specimens were partially immersed in 10% sodium chloride (NaCl) solution.

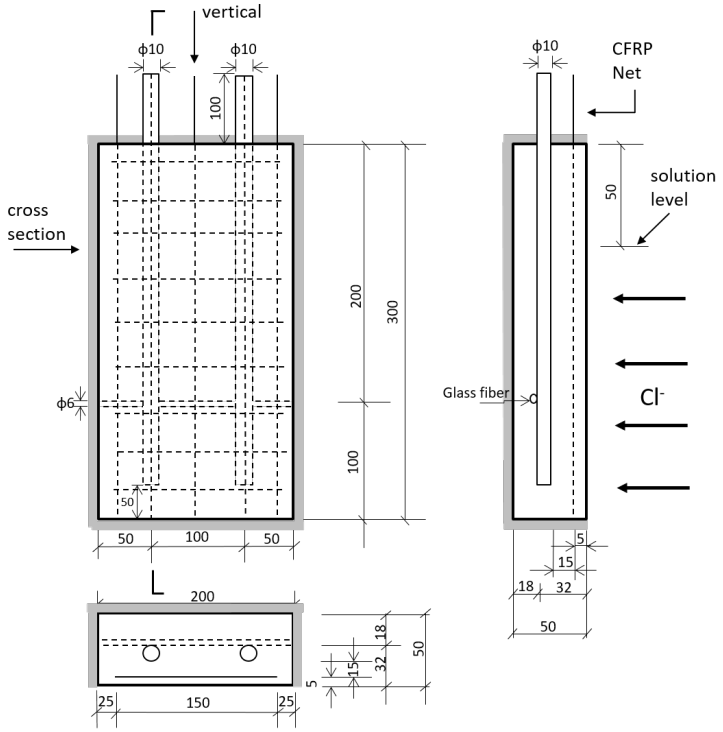

Figure 3.3: 3-view drawing of the mortar specimen. The solution level and the direction of chloride ingress are marked by arrows. Two cutting directions, cross section and vertical, are also indicated by arrows. All values are in mm.

3.2.3 Concrete specimen

For the corrosion monitoring, there were two types of specimens: test specimens and dummy specimens. Figure 3.4 illustrates the dimensions of the concrete test specimen, which contains one ribbed steel bar as cathode. For the chloride profiling, dummy specimens were used, which contained no steel bar. Figure 3.5 shows an image of a dummy specimen. The dimensions of the dummy specimen were 100 mm in diameter and 45 mm in height. All surfaces were covered with epoxy except the exposure surface.

The condition of the ribbed steel bar was as-received, without any chemical cleaning, as shown in Figure 3.6. The total length of the steel bar was 150 mm and 100 mm were cast inside the concrete with a pre-drilled hole at the top part for a cable connection. The part exposed in air was wrapped with electrical tape to prevent condensation and corrosion before they were ready for casting. After the test specimens were cast and hardened, the top surface of each test specimen, especially where the rebar was located, was immediately coated with epoxy to prevent unwanted corrosion.

The immersion solution was a 6% NaCl solution. The test specimens were partially immersed and the dummy specimens were completely immersed.

All test specimens and dummy specimens were preconditioned prior to the actual test. The purpose of the preconditioning was to accelerate the chloride penetration process, which was fast in the beginning due to capillary suction from drying. All the specimens were sealed in a box with RH 11% (potassium acetate saturated

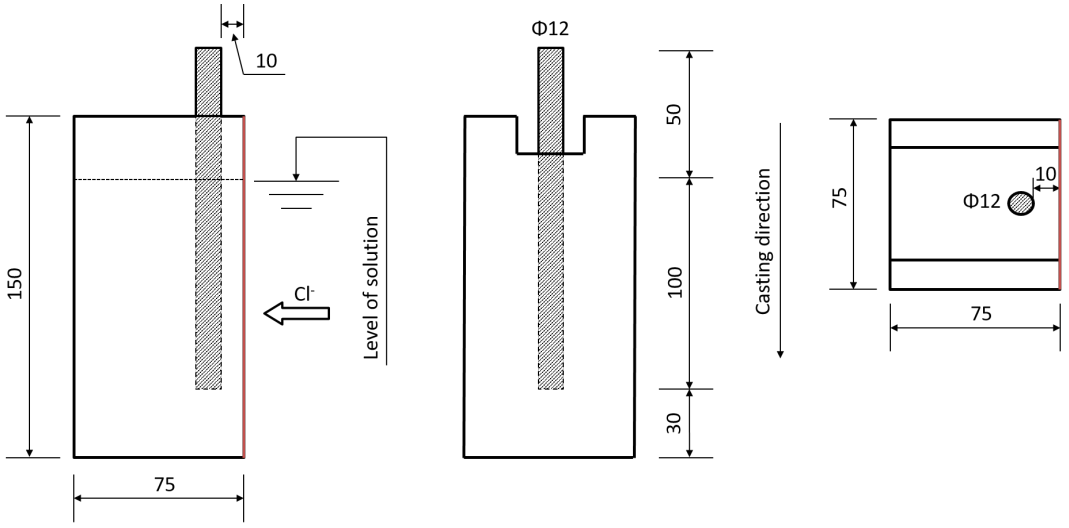

Figure 3.4: Dimensions of the concrete test specimen. Red lines indicate the exposure surface.

solution) environment and sodium hydroxide tablets for absorbing carbon dioxide. The preconditioning was terminated after five to six weeks, once the drying depth was reached, approximately 7 mm after 24 h submerged in the immersion solution. The drying depth was checked by silver nitrate spray after 24 h of being submerged in the immersion solution, as shown in Figure 3.7.

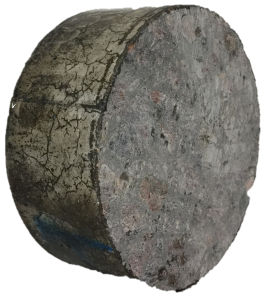

Figure 3.5: Image of a concrete dummy specimen

Figure 3.6: An image of as-received steel reinforcement

Figure 3.7: Preconditioning check.

3.3 Experiment set-up

3.3.1 Electrical set-up

Figure 3.8 illustrates the experimental set-up for the accelerated tests applied to the paste and mortar specimens. A constant current was applied to the specimens by a galvanostatic power supply. The current and potential between the cathode (steel) and the anode (CFRP) were monitored over the period of the experiment.

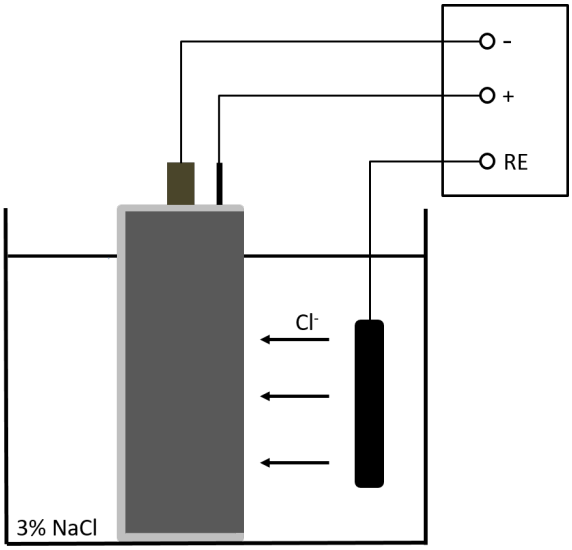

Figure 3.8: Experimental arrangement of the ICCP system. Steel as cathode is connected to negative terminal (–) and CFRP as anode is connected to positive terminal (+). RE represents the reference electrode. The direction of chloride penetration is indicated by arrows.

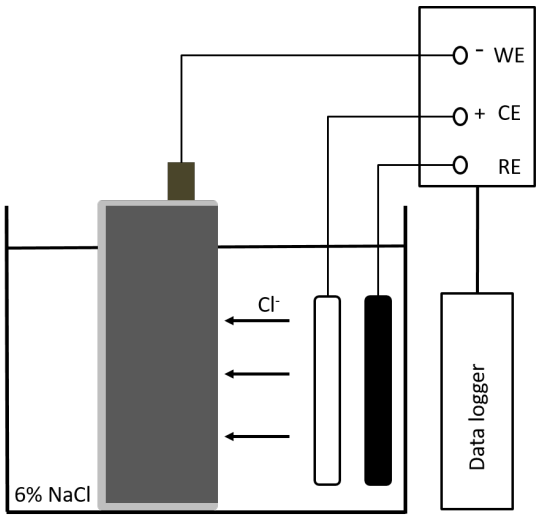

Figure 3.9: Experimental set-up for corrosion monitoring. Steel as cathode is connected to negative terminal (–) as working electrode (WE) and MMO-Ti mesh is connected to positive terminal (+) as counter electrode (CE). RE represents the reference electrode. The direction of chloride penetration is indicated by arrows.

Figure 3.9 illustrates the experimental set-up for corrosion monitoring, with steel as the working electrode (WE), and titanium net as the counter electrode (CE) and reference electrode (RE). A constant current was applied to the test specimens. Depending on the current density, the specimens were grouped into separate boxes, with one box for the reference group (no current applied), one box for the 1 mA/m^2 group, two boxes for the 2 mA/m^2 groups, and one box for the 5 mA/m^2 group. The current supply was on for 23 hours and off for 1 hour. Data loggers recorded hourly the potential response under the normal condition. During the corrosion measurement, the data logger made its recordings more frequently. A description of the measurement procedure will be given in Section 4.4.1.

3.3.2 Accelerated tests

The levels of current densities used in the accelerated tests were defined as low, medium, and high. They are shown in Table 3.3. The current densities were expressed with respect to the anode surface. Unless specially mentioned, the current densities of the anode surface (i_{an}) are used throughout this study.

It is worth mentioning that the maximum current density for cathodic protection in practice is 108 mA/m^2, as recommended by NACE Standard Practice *Impressed current cathodic protection of reinforcing steel in atmospherically exposed concrete structures*. Hence, the accelerated tests will cause extra damage to the ICCP system due to the application of significantly higher current densities, and this should be taken into consideration for design when converting results from accelerated tests.

Table 3.3: Defined acceleration levels of current densities used in the accelerated tests

Acc. level	Current density (i_{an})	Remarks
High	>1 A/m^2	fast reactions; uncertainty increases
Medium	0.25 A/m^2 $\sim$ 1 A/m^2	intermediate accelerated effect
Low	<0.25 A/m^2	no Cl_2 gas if $E_{an} < 1.1V_{SCE}$

Table 3.4 gives the details of the accelerated tests for paste specimens aimed at the investigation of the anode–paste interface. The accelerated test was planned for 37 days. However, two of them were terminated two days earlier, due to the negative effects of significantly high current densities.

Table 3.4: Experimental program of accelerated tests for the anode–paste interface study

Group	i_{an} (A/m^2)	Duration (day)	Acceleration level
P-i3-a	2.1	35[a]	High
P-i3-b	2.1	37[c]	High
P-i6-a	4.0	35[b]	High
P-i6-b	4.0	37[c]	High

[a]terminated due to surface cracks and spalling;
[b]terminated due to damage to anode–cable connection;
[c]terminated as planned;

Table 3.5 presents the details of the accelerated tests for the service life analysis, which contained both paste and mortar specimens. Different levels of constant currents were applied by several galvanostatic power supply units. Here, the test specimens were further divided into groups, including an indication of the applied current and binder type in the group names.

Table 3.5: Experimental set-up for service life modeling

Group	Number of specimens	i_{an} (A/m^2)	Duration (day)	Acceleration level
P-i6	4	4.0	20	High
P-i3	7	2.1	37	High
P-i0.3	2	0.2	377	Low
M-F-i40	3	1.0	86	Medium
M-G-i40	3	1.0	86	Medium
M-F-i20	2	0.5	103	Medium
M-G-i20	4	0.5	103	Medium
M-F-i10	4	0.25	200	Medium
M-G-i10	2	0.25	200	Medium
M-30D	3	5.0	30	High
M-60D	3	5.0	60	High

Chapter 4

Characterization and measurement methods

This chapter describes the characterization tools used for chemical and microstructural analysis, the methods for calculating the calcium leaching degree and leaching depth, as well as the measurement and fitting procedures for the corrosion monitoring.

4.1 Analytical instruments

After the accelerated tests, the treated paste specimens were prepared for topographical and chemical analysis. Topography imaging and elemental analysis were carried out by a scanning electron microscope with energy dispersive X-ray spectroscopy (SEM-EDS). The determination of the distribution of chemical elements over the cross-section of the specimens was carried out by laser ablation-inductively coupled plasma-mass spectroscopy (LA-ICP-MS) using line-scanning mode.

The analyses of the crystal phases and molecular interactions were conducted by X-ray diffraction (XRD) and nuclear magnetic resonance (NMR), respectively. Powder samples were extracted from the degradation zone by carefully scraping them from the bulk specimen. The collected powder was ground and stored in a CO_2-free environment.

4.1.1 LA-ICP-MS

Laser ablation-inductively coupled plasma-mass spectroscopy quantifies the longitudinal changes in the distribution of elements. The laser ablation analysis was performed using a New Wave NWR213 laser ablation system coupled to an Agilent 7500a quadrupole ICP-MS.

A Large Format Cell held samples up to a size of 10 cm × 10 cm, combined with a 1 cm diameter ablation chamber at the ablation region, enabling fast washout anywhere in the sample chamber. A 30 μm laser spot size, beam energy density of about 6 J/cm^2, and a repetition rate of 10 Hz was used in line-scanning mode (scan speed 60 μm/sec). The samples were dried and fine polished prior to measurements.

Calibration was performed by frequently measuring the glass standard SRM NIST 610 using the values of Jochum et al. (2011). Each measurement consisted of 30 s background followed by 400 s of signal collection. Dwell times were 20 ms.

4.1.2 SEM-EDS

An FEI Quanta ESEM 200 equipped with a field emission gun and an Oxford Inca EDS system was used to perform the analysis. The samples were vacuum dried and fine polished prior to analysis. The elemental compositions were examined by an integrated energy dispersive spectrometer (EDS) in high vacuum mode. The detection limits were about 0.1% with EDS (1000 ppm). The accelerating voltage was 15 to 20 kV.

4.1.3 NMR

^{29}Si solid state nuclear magnetic resonance (NMR) under magic angle spinning (MAS) was used to gain information about the silicate species present. Single pulse experiments with an excitation pulse of 25° and a repetition time of 30 s were recorded at an MAS rate of 15 kHz using a 3.2 mm double resonance MAS probe at 14.7 T (Agilent Inova).

It is well established that a ^{29}Si spectrum of the silicate anion is represented in the range of −70 ppm to −76 ppm for Q^0 (monomer), −78 for Q^1 (dimer or end group in a chain), −81 to −85 for Q^2 (chain), −93 to −102 for Q^3 (branched structure) and −107 to −115 for Q^4 (networked structure) (Matsushita et al. 2004; Kim et al. 2012; Kurumisawa et al. 2013). The average degree of C-S-H connectivity $\bar{n}$ is calculated by (Le Saoût et al. 2006)

$$\bar{n} = \frac{Q^1 + 2Q^2 + 3Q^3}{Q^1 + Q^2 + Q^3}. \tag{4.1}$$

where a higher value of $\bar{n}$ represents a higher degree of polymerization of the C-S-H.

The mean chain length (MCL) or number of SiO_4 tetrahedra in the C-S-H can be calculated from Richardson's equation (Richardson 1999)

$$MCL = \frac{2 \times (Q^1 + Q^2)}{Q^1}, \tag{4.2}$$

where the relative proportions of silicon associated with the Q^n units were determined by deconvolution of the spectra and measurement of the area associated with each peak using a curve-fitting technique.

4.1.4 XRD

Characterization of the crystalline phases in the cement paste was carried out by X-ray Diffraction (XRD). The measurements were performed by using 0.015° per step and a time step of 12 s, resulting in a total measurement time for each sample of 24 h.

4.2 Measurement of leaching degree

The leached calcium content of the paste specimens was characterized by LA-ICP-MS in line-scanning mode. The obtained raw data was signal intensity (cps) of each measured element plotted over time, which can be transferred to different oxide contents against the scanning distance. The leaching degree of calcium (σ_{L}) was defined as the percentage of CaO content loss, which was expressed by

$$\sigma_{\mathrm{L}}(\%) = \frac{\sigma_{\mathrm{leached}}}{\sigma_{\mathrm{initial}}} \tag{4.3}$$

where $\sigma_{\mathrm{leached}}$ is the integrated area of the leached zone and $\sigma_{\mathrm{initial}}$ is the integrated area of the sound zone.

4.3 Measurement of leaching depth

The leaching depth of the paste and mortar specimens was measured by optical microscope and image analysis.

The samples were sliced in the direction perpendicular to the anode. The image analysis of the anode–concrete interface was done by an image processing program. As shown in Figure 4.1, the area of dissolution can be distinguished by colors and defined by free-shape selection. After the area was selected, the value was calculated automatically with a pre-defined spatial scale.

The leaching depth was measured along the specimen (perpendicular to the CFRP anode) at intervals of about 5 mm. The result obtained for one specimen was an average value of all measured points. Because the shapes of the dissolution areas were irregular and different at each location, the normalized leaching depth d_{L} was defined as

$$d_{\mathrm{L}} = \frac{A_{leached}}{C_{anode}} \tag{4.4}$$

where $A_{leached}$ is the area of the leached zone and C_{anode} is the perimeter of the anode cross-section.

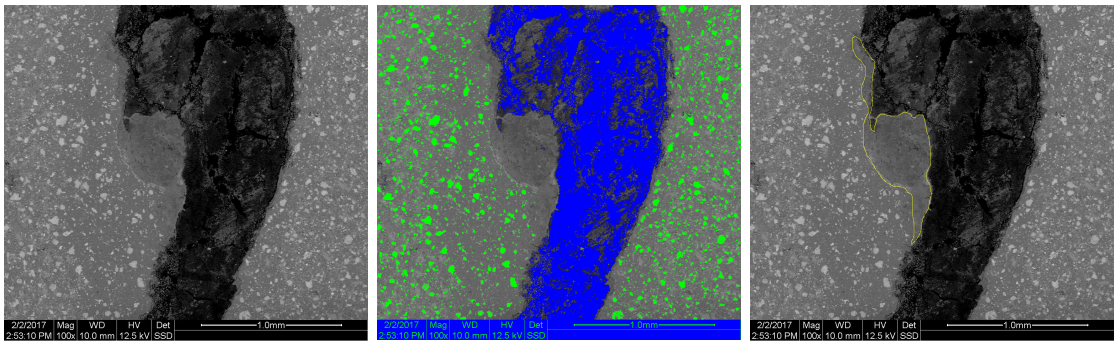

(a) Original (b) Color scale (c) Selected area

Figure 4.1: Example of image analysis of leached zone in paste specimen. Black part is the CFRP anode.

4.4 Corrosion monitoring

The method for corrosion monitoring contains two parts: determining the onset of corrosion by monitoring the corrosion rate, and then calculating the chloride threshold content by fitting the chloride penetration profile.

4.4.1 Corrosion rate measurement

The reinforcement was polarized by a cathodic current for a short period of time. The resulting change in the electrochemical potential of the reinforcement was recorded as a function of the polarization time.

It is important that the response has to be stabilized to gain an accurate value of a maximum potential, E_{max}. Extrapolating or curtailing the measurement before an equilibrium value for E_{max} has been obtained may lead to errors in the calculation and evaluation of the polarization resistance, R_p, and the double layer capacitance, C_{dl}.

The potential response to the pulse at time t is expressed by

$$E_t = I_{app}\left[R_p\left(1 - exp\left(-\frac{t}{R_p C_{dl}}\right)\right) + R_\Omega\right] \tag{4.5}$$

where I_{app} is the applied current, R_p is the polarization resistance, R_Ω is the Ohmic resistance and C_{dl} is the double layer capacitance.

Equation 4.5 is based on a simple Randles model that represents the steel surface, the passivation layer, and the concrete (Newton and Sykes 1988). To gain a better

fitting result from the recorded response, an equivalent circuit containing three Randles circuits in series was adopted in this study, as illustrated in Figure 4.2. Thus, the potential response is written as

$$E_t = I_{app}\left[\sum_{i=1,2,3} R_i\xi_i\left(1 - exp\Big(-\frac{t}{R_i\xi_i C_{dl}}\Big)\right) + R_\Omega\right] \tag{4.6}$$

where R_Ω was measured manually before the polarization test.

The procedure for measuring the corrosion rate for the reference group was different from that for the other test groups. For the reference group, the polarization current was 20 μA and the polarization time was 15 min. Each measurement included a few seconds before the polarization as a baseline, 15 min of polarization, and 15 min of depolarization. The response was recorded every second.

The test groups were under a daily cycle of 23 h polarization and 1 h depolarization. During their corrosion rate testing, the daily cycle remained the same, only the recording frequency was set to every 10 s for 3 h, to capture the changing response during the 1 h polarization and followed by 2 h depolarization.

After the polarization and depolarization response had been recorded, an exponential fitting procedure was adopted to calculate R_p and C_{dl}, by

$$R_p = \sum_{i=1,2,3} R_i\xi_i \tag{4.7}$$

where the ξ_i are fitting parameters and it should be noted that ξ_i, R_p and C_{dl} are fitted and calculated based on the polarization curves. The fitting results based on the depolarization curves have been reserved for further analysis and are not included in this thesis.

The corrosion rate, I_{cor}, can then be calculated by

$$I_{cor} = \frac{\beta_a\beta_c}{2.3R_p(\beta_a + \beta_c)} = B/R_p \tag{4.8}$$

where B is the Stern–Geary constant. A value of 26 mV has been adopted in this study (Morris et al. 2002; Pech-Canul and Castro 2002).

In order to determine the corrosion current density, i_{cor}, the surface area of the steel, A, has to be defined:

$$i_{cor} = I_{cor}/A_{immersed} \tag{4.9}$$

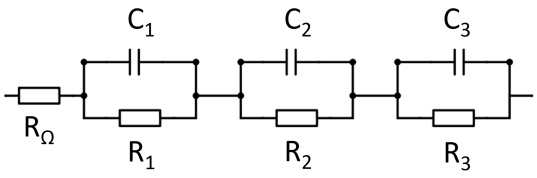

Figure 4.2: An equivalent Randles circuit.

where $A_{immersed}$ is the surface area of steel that has been polarized, which in this work was roughly calculated as the surface area of the steel that was immersed in solution.

4.4.2 Chloride penetration profile

The chloride penetration profiles of the dummy specimens were measured at a series of exposure times. Concrete powder were ground at different penetration depths. The acid-soluble chloride was extracted in accordance with *AASHTO T 260-97*. The total chloride was determined by chemical titration with 0.01 mol/l silver nitrate solution with an automatic potentiometric titrator Metrohm 736 GP Titrino. It should be noted that the chloride penetration profile is not a traditional diffusion profile, because it contains capillary suction at the beginning due to the preconditioning procedure for shortening the experimental time.

The surface chloride content, C_s, and the apparent diffusion coefficient, D_a, can be obtained by regression analysis of the measured chloride profiles using Equation 4.10:

$$C(d,t) = (C_s - C_i) \times \left[1 - erf\left(\frac{d}{2\sqrt{D_a t}}\right)\right] + C_i \tag{4.10}$$

where $C(d,t)$ is the chloride content (wt% of cement) at penetration depth d at exposure time t, and C_i is the initial chloride content in the cement, which is 0.01% by weight of cement.

To estimate the apparent coefficient at a certain corrosion onset, D_{acr}, it has to be calculated between two known D_a (obtained from measured chloride profiles) and interpolated using the age factor, n (Boubitsas and Tang 2013):

$$n = -\frac{\ln(D_{a1}/D_{a2})}{\ln(t_1/t_2)} \tag{4.11}$$

where D_{a1} and D_{a2} were known from measured chloride profiles obtained by curve fitting using Equation 4.10, and t_1 and t_2 were their corresponding exposure times, that should be chosen as close as possible to t_{cor}.

Then D_{acr} can be calculated using

$$D_{acr} = D_{a1}\left(\frac{t_{a1}}{t_{cor}}\right)^n \tag{4.12}$$

Thus, the calculation of C_{cr} is

$$C_{cr} = C(d_{cv}, t_{cor}) = (C_{s,avg} - C_i) \times \left[1 - erf\left(\frac{d_{cv}}{2\sqrt{D_{acr} t_{cor}}}\right)\right] + C_i \tag{4.13}$$

where d_{cv} is the cover depth of the concrete test specimen, t_{cor} is the corrosion onset determined from the corrosion monitoring, and $C_{s,avg}$ is the average of the two curve-fitted values.

Chapter 5

Results

5.1 Durability of CFRP anode

Figure 5.1 shows the SEM results of the undamaged carbon fiber after the accelerated test for 60 days with a current density of 4.6 A/m^2, in which the polymer matrix disappeared due to oxidation, leading to a higher porosity at the anode. It was demonstrated that carbon fiber can remain undamaged under high current densities with no obvious material loss, which indicates that its functionality as anode was not compromised under ICCP.

To converse the total charge density (60 days $\times$ 4.6 A/m^2) to a condition using a current density of 5 $mA/^2$, even with a linear relation, the estimated equivalent service life would be about 150 years, which has successfully proven the viability of using CFRP mesh as anode material for cathodic prevention applications.

5.2 Degradation of the anode–concrete interface

5.2.1 Untreated reference sample

A carbon fiber thread from mesh embedded in cement paste without electrochemical treatment was used as a reference sample to investigate the chemical composition without the effect from an external electrical field. Figure 5.2 shows images of the cross section of the control sample. The dimensions of a carbon fiber thread at the widest and longest points were about 3 mm and 0.6 mm, respectively.

Table 5.1 presents the chemical analysis of the control sample using LA-ICP-MS compared with the clinker compositions that are provided by the manufacturer. The LA-ICP-MS results showed good precision for the calcium and silicon contents, which were the main elements for the later investigation in this work. The concentrations of sodium and chloride were not comparable with the clinker values

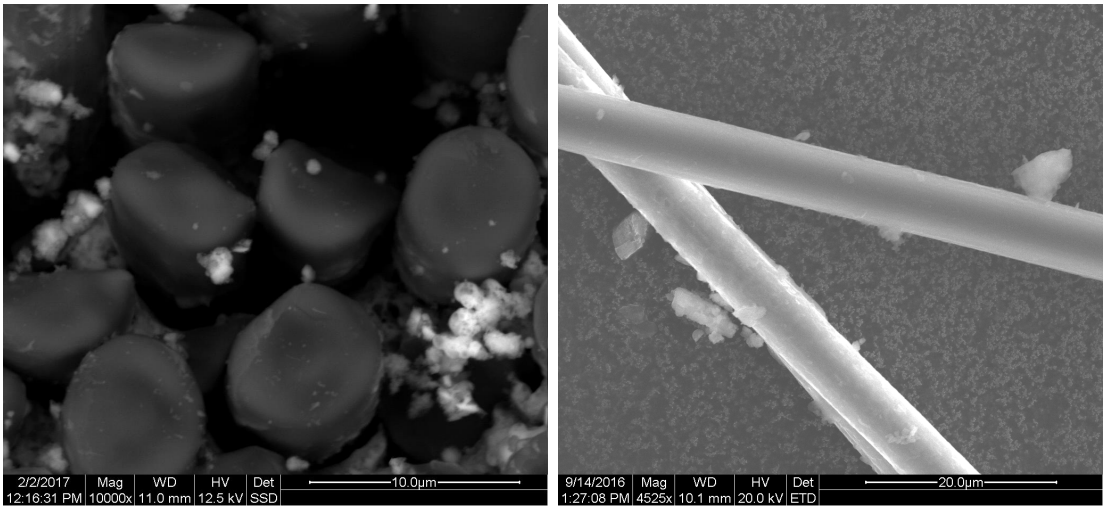

(a) Image of the cross-section of CFRP (b) Image of two single fibers with smooth surface

Figure 5.1: Undamaged CFRP anode after the accelerated test. The white crystals appearing in the corner in (a) and next to the fiber in (b) are potassium (K^+) and chloride (Cl^-) enriched phases, which are formed during the drying process of sample preparation.

because the control sample was immersed in 10% NaCl solution for a month before the test.

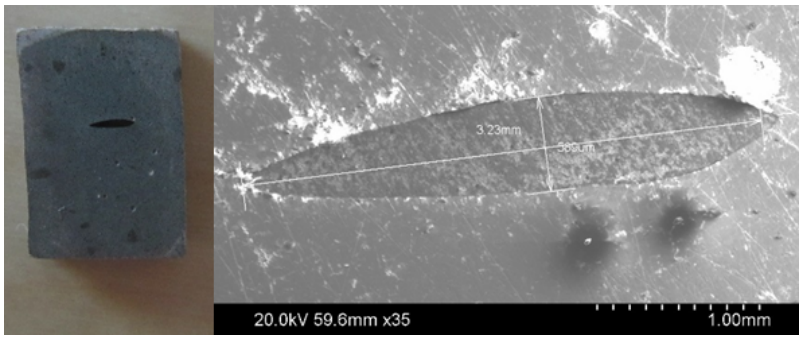

Figure 5.2: Image of the cross section of a control sample.

5.2.2 Degradation pattern at the anode–concrete interface

Figure 5.3 presents the degradation pattern after the accelerated test and the SEM image on the right side also confirms the different phases formed around the anode. The size of each leached zone was from 0.5 to 2 mm around the anode. This specimen was subjected to a current density of 800 mA/m^2 for 60 days.

When high levels of current densities were applied, the degradation zone showed a distinctive change of color, specially at the top part of a specimen. Figure 5.4 shows the typical leaching pattern of the paste groups at the top, middle and bottom part of the specimen after accelerated tests. Around the CF anode (the black part), the most severe leached cement paste showed distinguishing white color, such as in

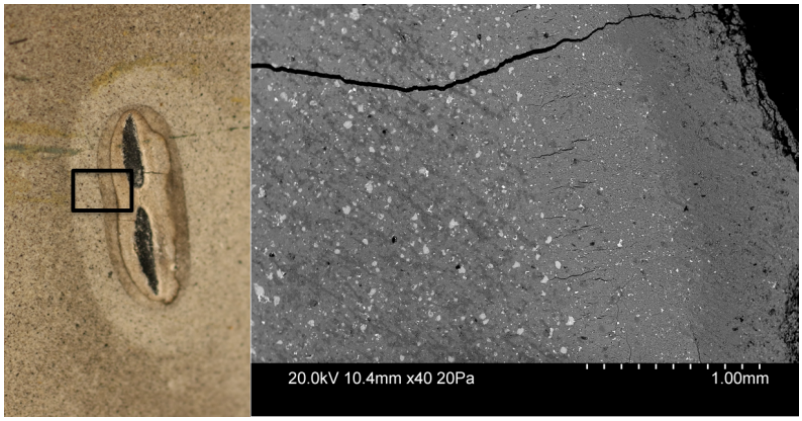

Figure 5.3: Images of the ring pattern around the anode. The crack through the area was formed after the experiment, caused by drying.

Figure 5.4a and 5.4d. The less severely leached paste showed white or gray color around the anode, both of which can be easily identified. In the case such as in Figure 5.4b and 5.4c, an open space between the anode and the cement paste has been observed. As shown in Figure 5.4c, the widest gap between the anode and cement paste was 0.09 mm measured by an image analysis program. A similar phenomenon has been reported when using titanium wire as an anode, for which the disappearing material was $Ca(OH)_2$ crystals (Polder et al. 2002).

Figures 5.5 and 5.6 present the typical leaching patterns of the mortar groups at the solution level, the middle, and the bottom part of the specimen.

In general, the most severe degradation occurred at the solution level, where the specimen has access to both moisture and oxygen. Therefore, the anode reactions can proceed rapidly without hindrance. Below the solution level, the specimens were completely immersed and the availability of oxygen was limited compared to that at the solution level. Hence, the leaching area was less and, moreover, the degree of leaching was also less severe, which is indicated by the fact that the discolored area was not as distinct as that at the solution level.

Table 5.1: LA-ICP-MS chemical analysis of the control sample compared to clinker compositions provided by the manufacturer

Composition	Clinker (wt% of cement)	LA-ICP-MS analysis (wt% of cement)
CaO	64.1	64
SiO_2	22.5	24
Al_2O_3	3.1	3.5
Fe_2O_3	4.0	3.0
MgO	1.3	1.1
Na_2O	0.12	2.2
K_2O	0.58	0.3
SO_3	2.6	–
Cl	0.01	3.4

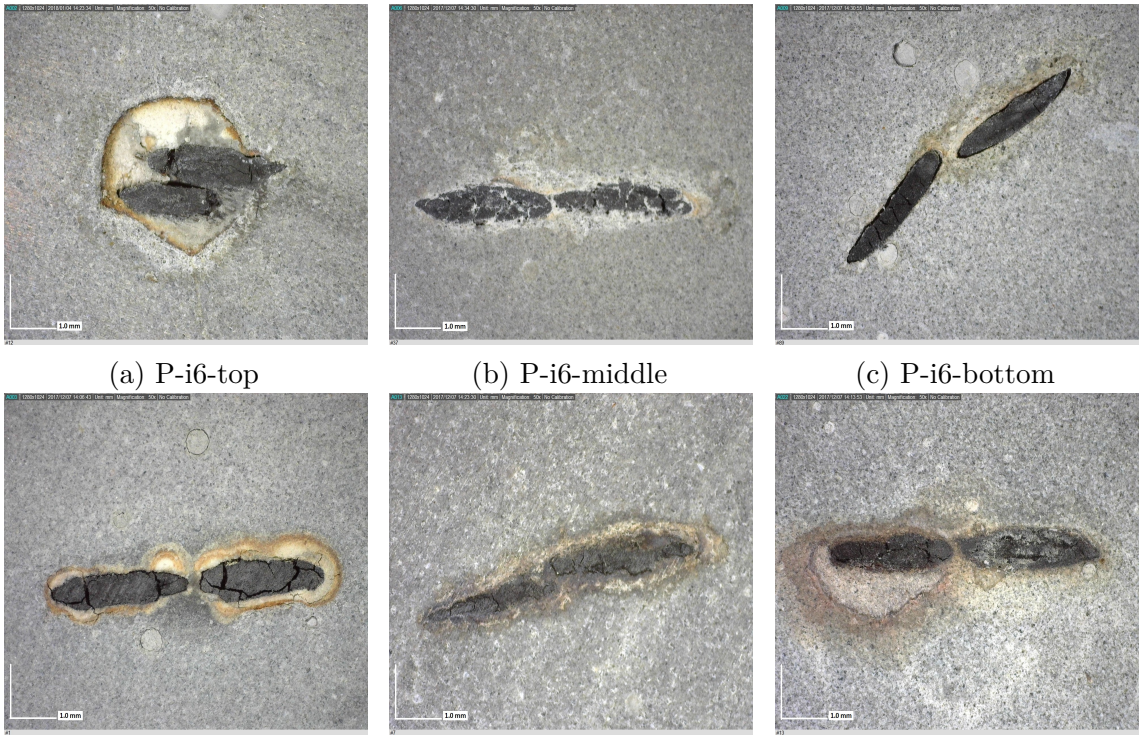

(a) P-i6-top (b) P-i6-middle (c) P-i6-bottom

(d) P-i03-top (e) P-i03-middle (f) P-i03-bottom

Figure 5.4: Typical leaching patterns of specimen's cross section for paste groups.The current density is listed in Table 3.5.

It has also been observed that the leaching areas of the M-G groups were less than those of the M-F groups. For example, in the M-G-i10 group in Figures 5.6g–5.6i, both the area and the color difference of the leached concrete became clearly less than those of the M-F-i10 groups, as shown in Figures 5.5g–5.5i. Table 5.2 lists the measured average leaching depths after the accelerated test.

Because the mixture of the M-G groups contained 25% slag, the microstructure of the cement paste is denser than for Portland cement concrete with the same w/c ratio (Chen 2006). Thus, the ion diffusion rates are lower, which partially explains the good performance of slag cement concrete against chloride ingression (Daube and Bakker 1986). However, the low ion diffusion rates in this experiment limit the chemical reaction rate, because this depends on the availability of active ions. This could explain why the degradation was less severe in the M-G groups than in the M-F groups, especially under low current densities.

5.2.3 Leaching depth of the degradation zone

It is worth mentioning that the equivalent CaO content in the paste specimens was three times that of the mortar specimens, as listed in Table 3.2. Therefore, the leaching depths of the paste and mortar specimens can not be simply compared with each other. Figure 5.7 summarizes the leaching depths of two paste groups, Pi-3 and

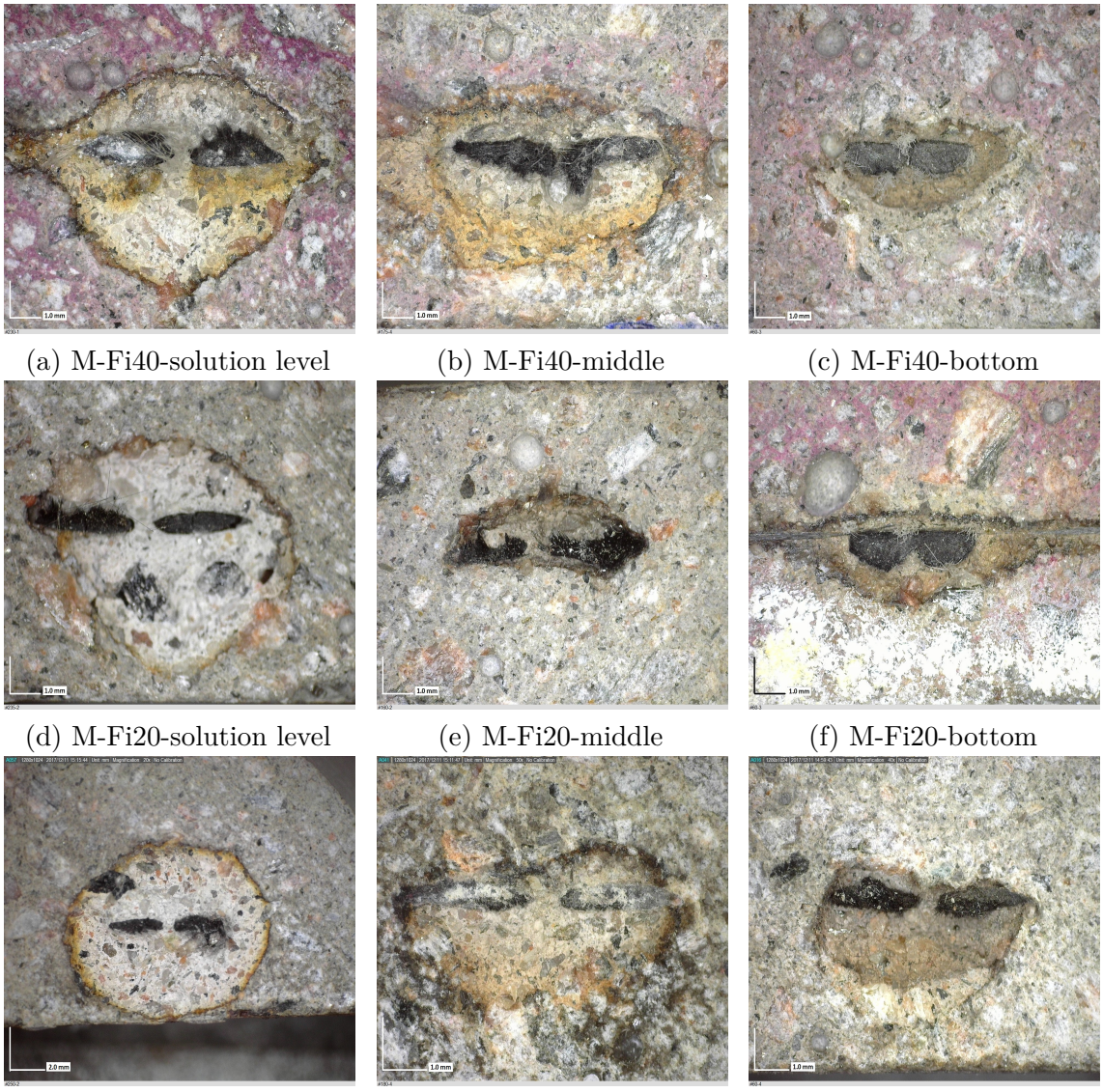

(a) M-Fi40-solution level (b) M-Fi40-middle (c) M-Fi40-bottom

(d) M-Fi20-solution level (e) M-Fi20-middle (f) M-Fi20-bottom

(g) M-Fi10-solution level (h) M-Fi10-middle (i) M-Fi10-bottom

Figure 5.5: Typical leaching patterns of specimen's cross section for M-F groups. Pink color implies sound concrete indicated by phenolphthalein pH indicator. The current density is listed in Table 3.5.

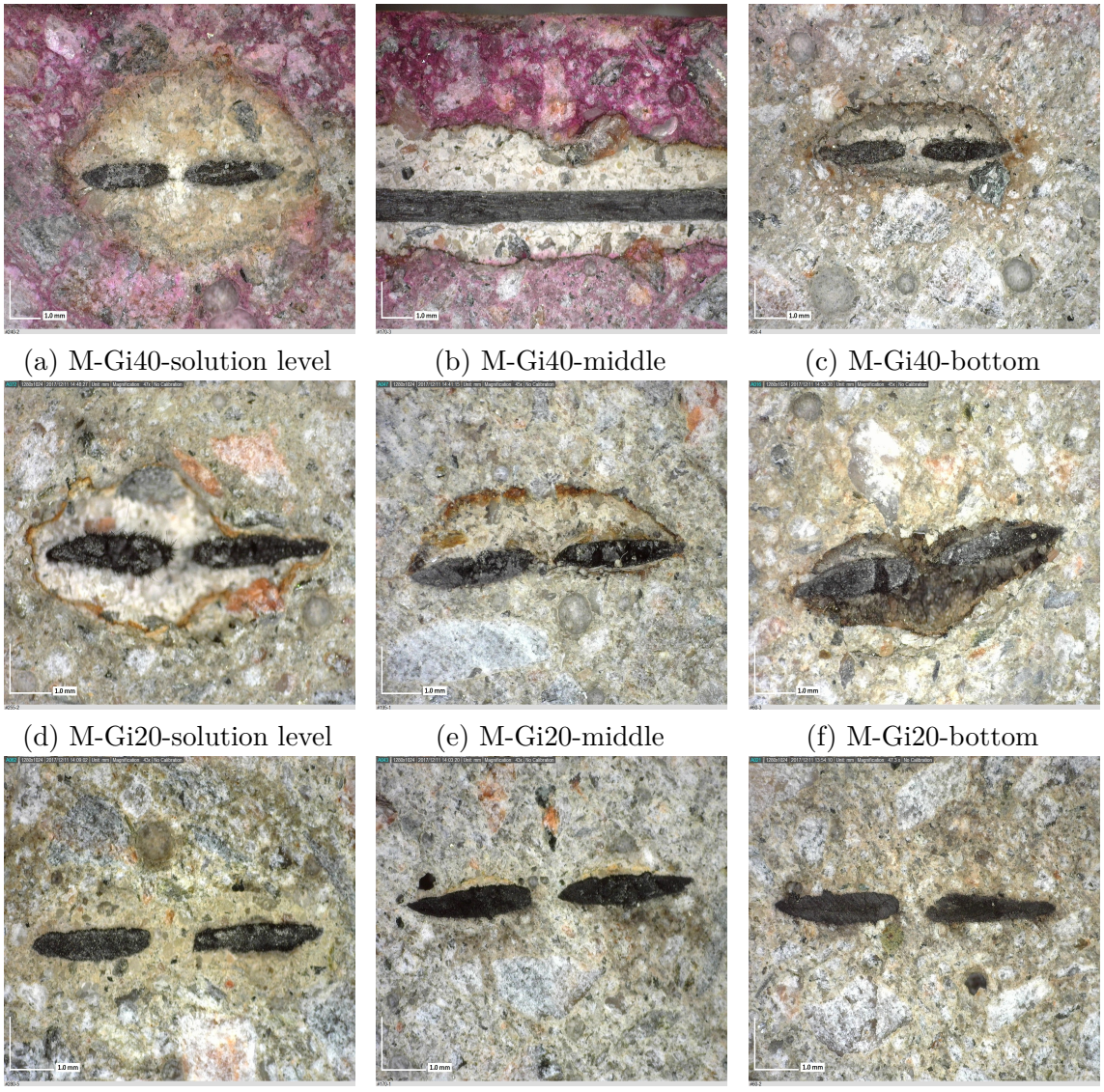

(a) M-Gi40-solution level (b) M-Gi40-middle (c) M-Gi40-bottom

(d) M-Gi20-solution level (e) M-Gi20-middle (f) M-Gi20-bottom

(g) M-Gi10-solution level (h) M-Gi10-middle (i) M-Gi10-bottom

Figure 5.6: Typical leaching patterns of specimen's cross section for M-G groups. Except image (b) is from vertical cutting. Pink color implies sound concrete indicated by phenolphthalein pH indicator. The current density is listed in Table 3.5.

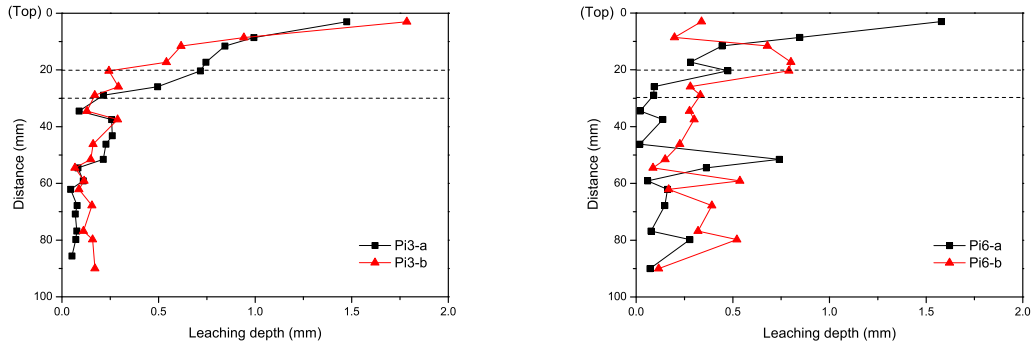

(a) Pi-3 group (b) Pi-6 group

Figure 5.7: Leaching depth of group Pi-3 and Pi-6. Dashed lines indicate the solution level, which varies between 20 mm and 30 mm from the top.

Pi-6. The position of the solution level was approximately 20 to 30 mm from the top. Most of the calcium dissolution took place at and above the solution level. Below the solution level, the degradation zones tended to be smaller and evenly distributed. Moreover, the Pi-3 group showed a better pattern than the Pi-6 group, implying that a current density of 4 A/m^2 could cause extra damage and increase the uncertainty of the results.

5.2.4 Characterization of calcium leaching

An elemental analysis was carried out by SEM-EDS at each leached zone, as illustrated in Figure 5.8. The result is given in Table 5.3: the Ca/Si (C/S) ratio decreased in the zone close to the anode and the Na/Si ratio increased.

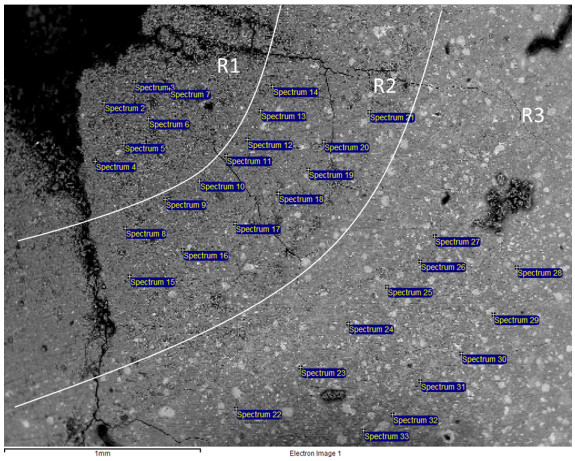

Figure 5.8: Back-scattered SEM spot analysis of the ring pattern formed around the anode.

Elemental analyses were also carried out at different heights of each specimen. Table 5.4 lists the C/S ratios measured by both SEM-EDS and LA-ICP-MS. The C/S ratio of the reference samples in tap water and in salt solution were also measured.

Table 5.2: Average leaching depths measured after accelerated tests

Group	d_{test} (mm)
P-i6	0.35
P-i3	0.33
P-i0.3	0.14
M-F-i40	1.17
M-G-i40	0.71
M-F-i20	1.09
M-G-i20	0.46
M-F-i10	0.81
M-G-i10	0.32

Table 5.3: Calcium and sodium content at each leached zone around the anode

Leached zone	C/S ratio	Na/Si ratio
Ring 1	2.63	0.20
Ring 2	3.50	0.11
Ring 3	5.88	0.07

The results obtained by SEM-EDS were generally lower than those from LA-ICP-MS. However, within each sample, the consistency of the measured values was relatively good. These make the SEM-EDS results suitable for comparison within one sample, while the LA-ICP-MS measurements were appropriate both for analysis within one and between several samples.

For specimen Pi-6-a, the C/S ratio of the unaffected zone was in good agreement with those of the reference samples. The C/S ratios of the degradation zone were smaller than those in the unaffected zone, according to both analysis techniques. The results from LA-ICP-MS gave a profile changing against the distance from the exposure surface, with the lowest value of 1.0 on average on the fitted curve at the position close to the anode, which was smaller than that obtained by SEM-EDS.

Table 5.4: Measured C/S ratios in reference and accelerated samples. LA-ICP-MS is in line-scanning mode. Results from SEM-EDS are presented by average values ± standard deviation.

Samples	LA-ICP-MS	SEM-EDS±St.Dev.	Remarks
Ref in tap water	3.1	2.9 ± 0.8	Avg. of 35 points
Ref in salt solution	3.1	2.3 ± 0.7	Avg. of 55 points
Pi-6-a unaffected zone	3.2	2.5 ± 0.9	Avg. of 24 points
Pi-6-a-H20 degraded zone	0.9	–	–
Pi-6-a-H43 degraded zone	0.8	–	–
Pi-6-a-H59 degraded zone	1.3	2.1 ± 0.1	Avg. of 26 points

Figure 5.9 presents the LA-ICP-MS measurements at different heights of the paste specimen P-i6-a. The fitted curves (dash-dot lines) of C/S ratios were analyzed to calculate the degree of calcium leaching. Figure 5.10 summarizes the calcium leaching degrees of the two paste groups. It can been seen that even for the specimens under strong current densities, there still remained about 20 % calcium content in the degradation zone, compared to 65% originally in the cement paste.

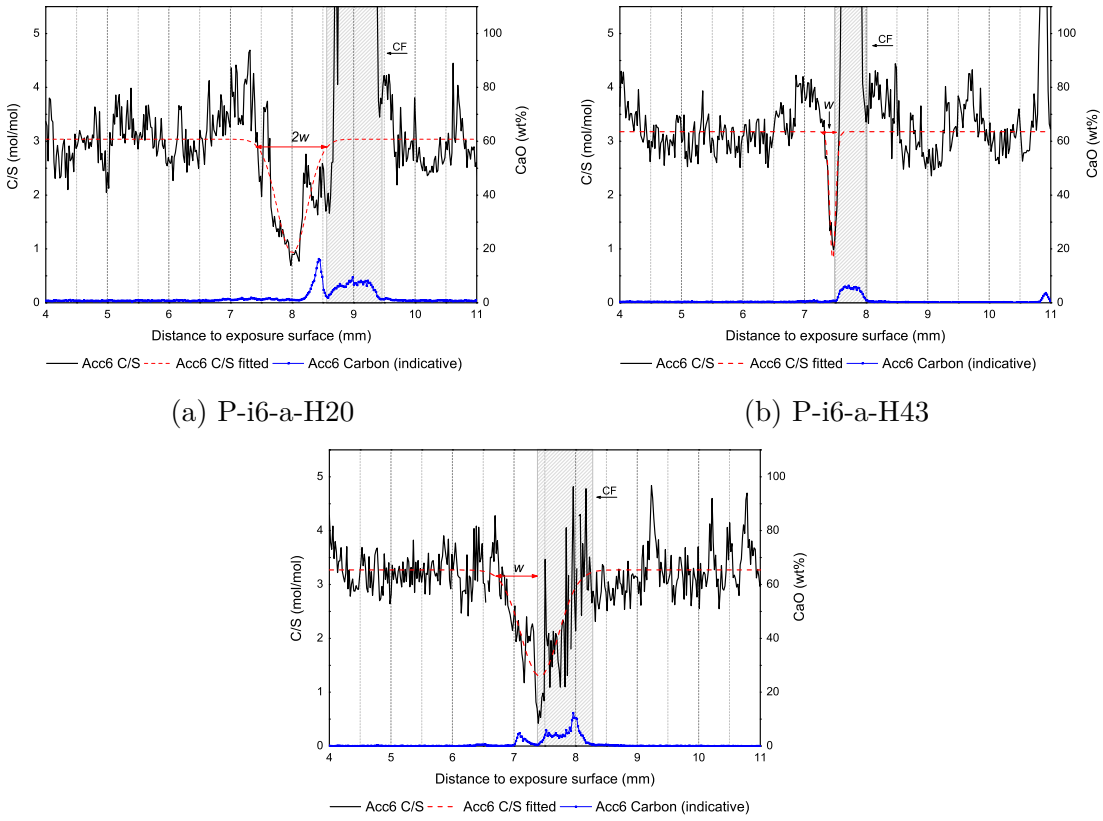

(a) P-i6-a-H20

(b) P-i6-a-H43

(c) P-i6-a-H59

Figure 5.9: Profile of C/S ratio in the accelerated sample P-i6-a at different heights. Dash-dot lines are fitted curves. Shadowed areas indicate the location of the CFRP anode. Arrow marks the thickness of decalcification.

Therefore, previous acid degradation models, if assuming the acid neutralization capacity is equal to its CaO content (Polder and Peelen 2011), may overestimate the amount of acid that can be neutralized by the cement paste.

5.2.5 Characterization of the degradation zone

Figure 5.11 illustrates the XRD analysis of the powders extracted from the reference and the degradation zones. The most apparent change between the reference and the degradation zones is the disappearance of Portlandite peaks and C-S-H peaks in the white zone. This is because the C-S-H gel phases were poorly crystallized, so they generally can be characterized in 2θ of 29° to 33° and about 51° (Babaahmadi 2015). The C-S-H gel phases present in the reference sample had almost disappeared in the degradation zone, indicating a high degree of calcium depletion and that mostly an amorphous silica-gel-like phase had formed. The major identified crystalline phase in the treated sample was gypsum, which was induced by the cement manufacturing process.

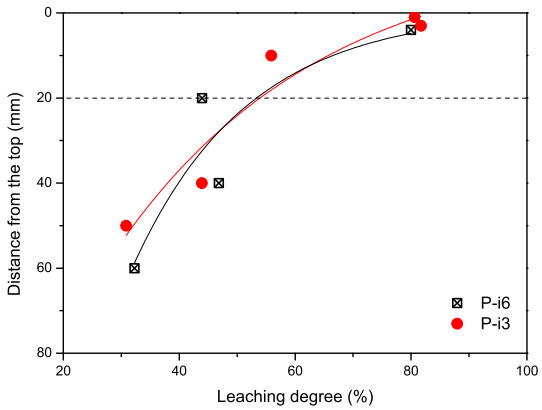

Figure 5.10: Leaching degree of paste groups P-i3 and P-i6. Dotted line indicates the solution level.

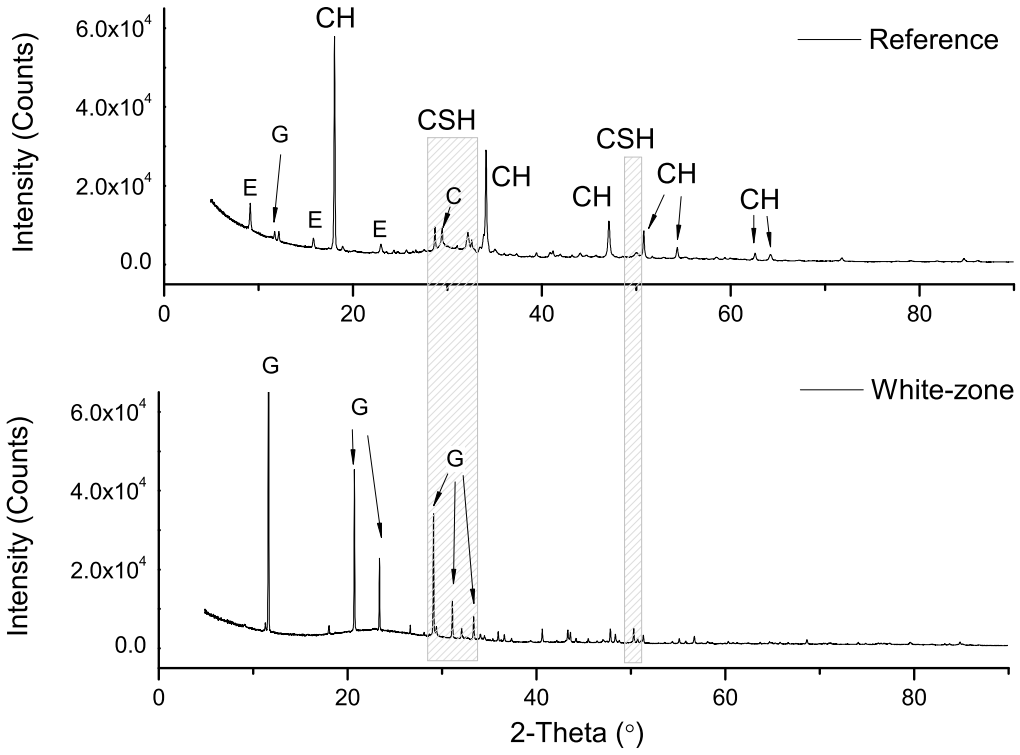

Figure 5.11: X-ray diffraction pattern of reference and the white-phase substance. Shadowed area indicates C-S-H phases. CH: Portlandite, $Ca(OH)_2$; CSH: calcium silicate and C-S-H gel; E: Ettringite; G: Gypsum; C: Calcite, $CaCO_3$.

The powder from the degradation zone was also examined by NMR analysis to provide information about the Si environment on an atomic scale. Figure 5.12 illustrates the chemical shift in the reference and the white-zone sample. As expected, in the reference sample only Q^1 (chain end) and Q^2 (within chain) peaks were visible, and neither Q^3 or Q^4 were observed, since chain structures were the major constituents in hardened cement paste (Kurumisawa et al. 2013). However, in the degradation zone, clear Q^3 and Q^4 peaks were observed, which indicated that branched and networked structures were formed due to a high degree of calcium depletion.

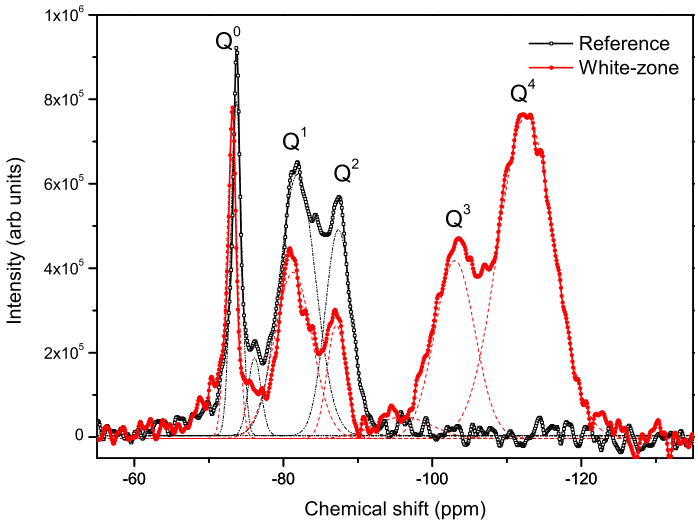

Figure 5.12: ^{29}Si solid state spectra of reference sample and white substance from the ring-pattern area.

The calculated connectivity $\bar{n}$ for the reference sample was 1.4 and for the degradation-zone powder was 2.1, indicating higher polymerization of C-S-H and a lower C/S ratio (Cong and Kirkpatrick 1996), which were confirmed by SEM-EDS and LA-ICP-MS analysis in Section 5.2.4. The average mean chain length (MCL) for the reference and the white-zone sample were 3.2 and 2.7, respectively, indicating that the chain lengths in the C-S-H gel were also reduced.

To summarize the results from the XRD and NMR, it can be suggested that the formed degradation zone showing a white color was a silica-gel like phase, which was amorphous and had developed branched and networked structures. The formation of such a phase was because of the high degree of calcium depletion as a consequence of the impressed current.

5.3 Failure analysis

5.3.1 Visual inspection of surface conditions

The current density used for groups ACC-M was about 5 A/m^2. Figure 5.13 shows the surface condition of specimens M-A1 to M-C1 after 30 days of accelerated testing. Surface damage was observed on specimens M-30D-P (OPC) and M-30D-G (PC+25%GGBS) at the position below and along the immersion line. However, specimen M-30D-F (PC+20%FA) still revealed a good surface condition, indicating that the fly ash additive probably has better homogeneity than slag.

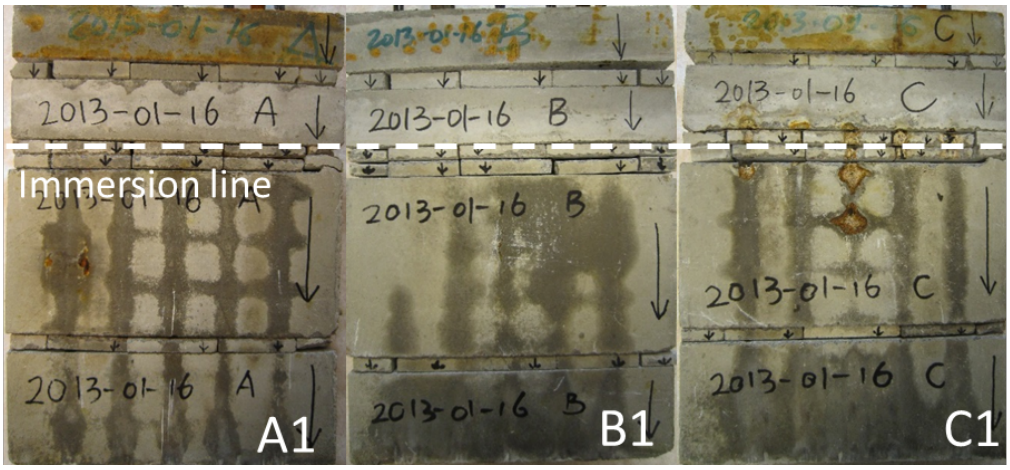

Figure 5.13: Group M-30D specimens after accelerated test of 30 days. Specimen A – OPC; B – PC+20%FA; C – PC+25%GGBS

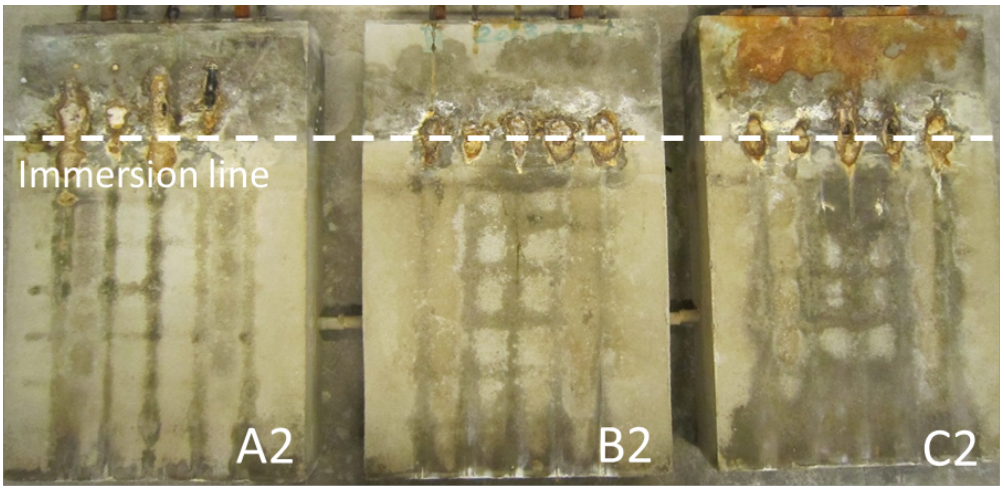

Figure 5.14: Group M-60D specimens after accelerated test of 60 days. Specimen A – OPC; B – PC+20%FA; C – PC+25%GGBS

Figure 5.14 shows specimens with the same mixture after 60 days of accelerated testing. All three specimens had surface damage along the immersion line, which

indicates that the area around the immersion solution, as in real cases representing the tidal zone and the splash zone, can be considered a critical area because it has a higher risk of leaching damage.

5.3.2 Loss of protection efficiency

Figure 5.15 presents the changes of cell potentials during the accelerated tests of the paste specimens. The maximum cell potential (E_{max}) was limited by the power supply unit. E_{max} for group P-i6 and P-i3 were about 18 V and for group P-i0.3 was about 9 V. The development of the cell potential has a one-step sigmoidal pattern for group P-i6 and P-i3, while for group P-i0.3 it has a two-step sigmoidal pattern. The turning points t_{crit} and t_{fail} are also marked in Figure 5.15: t_{crit} is a critical point before which the system undergoes drastic changes, which was used for the service life prediction model in this paper; t_{fail} is defined as a system failure point which indicates the system has lost its efficiency at protecting the reinforcing steel.

Mortar groups M-i40 and M-i20 were tested by medium-level current densities and group M-i10 by a low-level current density. Figure 5.16 presents the monitoring of the development of the cell potential of the mortar groups and the two turning points are also indicated. Their development showed a similar pattern as the paste groups P-i3 and P-i6.

Figure 5.17 shows the current decay of the P-i6 and P-i3 groups during the accelerated test. The currents were kept constant, for 12 days for the P-i6 group and 20 days for the P-i3 group, and then decreased dramatically to a level below 0.8 A/m^2 within several days. The applied current for group P-i0.3 was kept at 0.3 mA because the potential difference was not high enough to interrupt the circuit's galvanostatic performance.

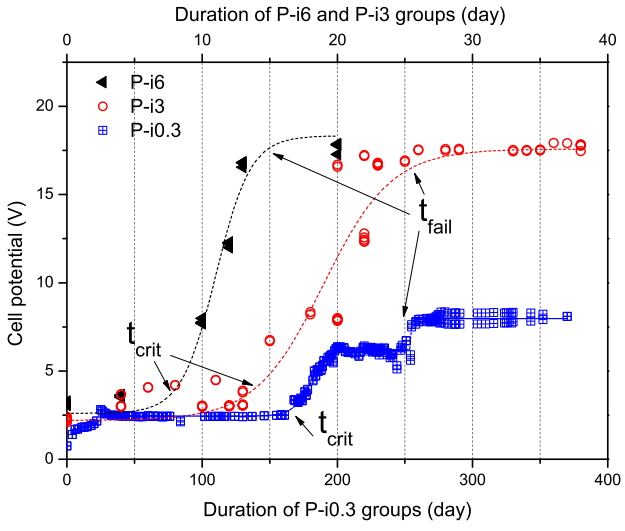

Figure 5.15: Potential monitoring of the paste groups. Dashed lines are fitted curves.

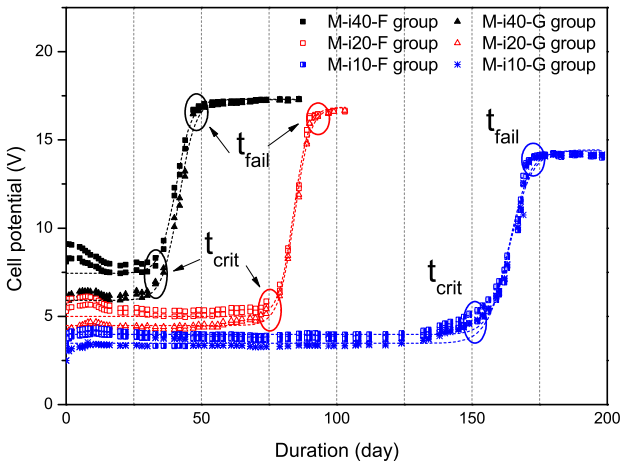

Figure 5.16: Potential monitoring of the mortar groups. Dashed lines are fitted curves.

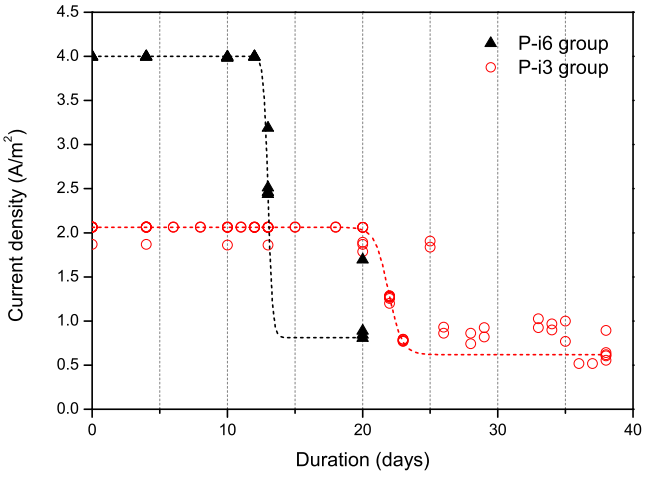

Figure 5.17: Current monitoring for the paste groups P-i3 and P-i6. Dashed lines are fitted curves.

Figure 5.18 presents the current decay of the mortar groups. As for the paste specimens, the current densities of the mortar groups were kept as the desired level for a certain period and then dropped dramatically, losing 50% of the current density within just a few days. Due to the limited experimental resources, the test for the mortar groups was terminated when the current densities lost about 50% compared to the starting value.

Figures 5.19 and 5.20 present the total charge passed during the accelerated test. The slope of the curves indicates the current densities. The changing point of the slope matched the time when the current density began to decrease, as well as t_{fail}, which was when the cell potential reached the maximum value.

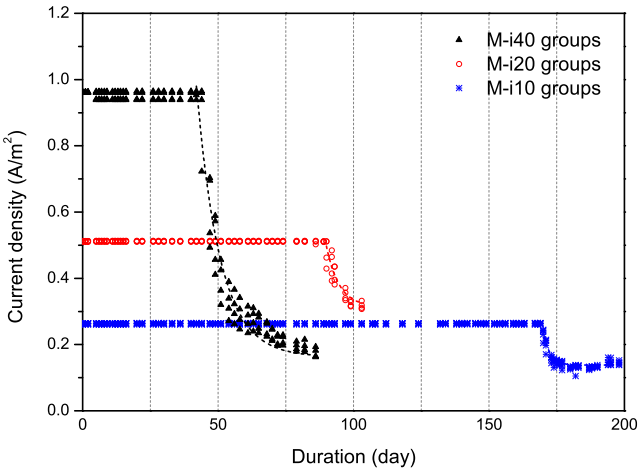

Figure 5.18: Current monitoring for the mortar groups. Dashed lines are fitted curves.

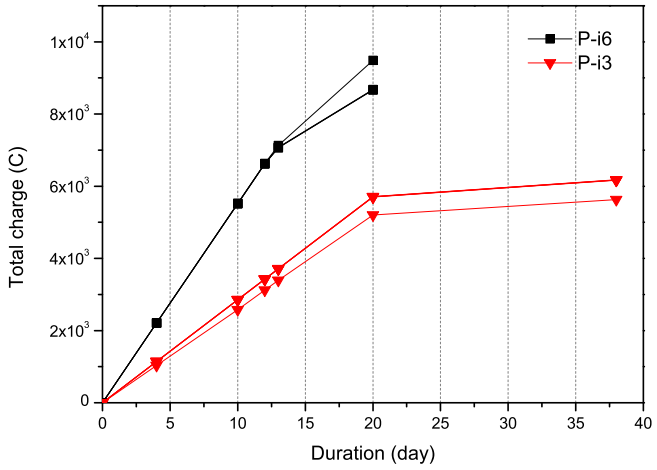

Figure 5.19: Evolution of the total charge of the paste groups P-i6 and P-i3.

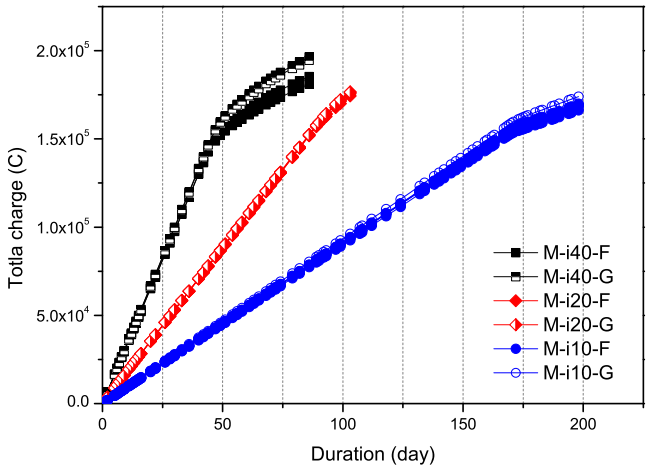

Figure 5.20: Evolution of the total charge of the mortar groups.

5.4 A conversion model for service life prediction

Table 5.5 lists the turning points t_{crit} and t_{fail} and the corresponding charge densities at each turning point: t_{crit} represents the service life of the system without compromising the efficiency of the protection, and is used as input data for the conversion model in this thesis; t_{fail} represents the failure point of the system, at which point the system can no longer fulfill its function.

The corresponding charge passed at t_{crit} suggests that the mortar specimens can tolerate more charge than can the paste specimens, because q_{crit} for the mortar specimens is on average higher than that for the paste specimens. The reason is probably that the current is more evenly distributed in the mortar specimens because of the mixture with fine sand.

Table 5.5: Turning points and their corresponding charge densities

		Critical point		Failure point	
Groups	i_{an} (A/m^2)	t_{crit} (day)	q_{crit} (kC/m^2)	t_{fail} (day)	q_{fail} (kC/m^2)
P-i6	4.0	6	2074	10	3412
P-i3	2.1	13	2284	20	3555
P-i0.3	0.2	161	2613	219	3554
M-i40-F	3.2	31	2530	44	3751
M-i40-G	3.2	32	2659	46	3990
M-i20-F	1.6	79	3279	90	3986
M-i20-G	1.6	79	3279	90	3990
M-i10-F	0.8	156	3554	180	4006
M-i10-G	0.8	159	3673	183	4075

Table 5.5 shows that t_{crit} is almost inversely proportional to the current density. However, when the current density was decreased by 50%, t_{crit} was increased to slightly more than its double. If this phenomenon can be determined quantitatively, it can be used to transfer the results of the accelerated test to the non-accelerated test by simply removing the acceleration effect and fitting the accelerated result to any specific current density level.

Figure 5.21 shows the turning point t_{crit} plotted against i_{an} in a log-log scale. The dotted lines are curves fitted by a power function $y = ax^{(-b)}$. The power function was rewritten as

$$t_{crit} = \frac{q_{crit}}{{i_{an}}^{b}} \tag{5.1}$$

where the parameter b is the acceleration factor.

Table 5.6 lists the acceleration factors for each type of binder. The fitting results show that all b factors are greater than one. That $b > 1$ indicates that specimens

exhibit a higher tolerance of charge passage if a lower current density is applied. The reason is because at lower current densities, the reactions are less aggressive and so allow the development of slow processes, such as dissolution and diffusion. Therefore, the more sever damage caused by the accelerated tests is de-escalated progressively by lowering the applied current density. Thus, a simple linear conversion from accelerated tests to a normal operation condition, such as in the case for cathodic prevention, will underestimate the predicted service life significantly.

Table 5.6: The acceleration factor of test results

Groups	b
Paste groups	1.06
Mortar M-F groups	1.07
Mortar M-G groups	1.08

Therefore, a nonlinear conversion model has been proposed for estimating the service life of the cathodic prevention condition using the results from accelerated tests, namely,

$$t_{nor} = t_{acc} \times \left(\frac{i_{acc}}{i_{nor}}\right)^{b} \tag{5.2}$$

where i_{acc} is the current density used in the accelerated tests; t_{acc} is the duration of the accelerated tests; i_{nor} is the current density in normal CP applications; and t_{nor} is the estimated service life of normal CP applications.

Figure 5.22 illustrates the estimated service life using the proposed power conversion model in comparison with a linear conversion, assuming the total charge is 3×10^6 C/m^2. The impact of the power model conversion is significantly greater when the

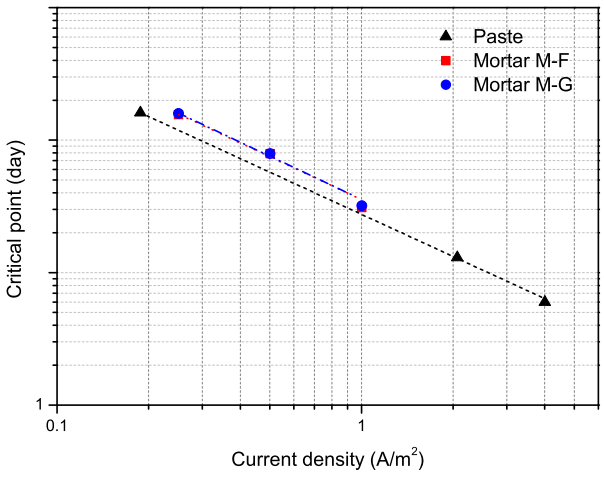

Figure 5.21: Critical turning point t_{crit} plotted against current density.

current density is reduced to below 10 mA/m^2, and is about 30% to 40% more than the results from the linear model.

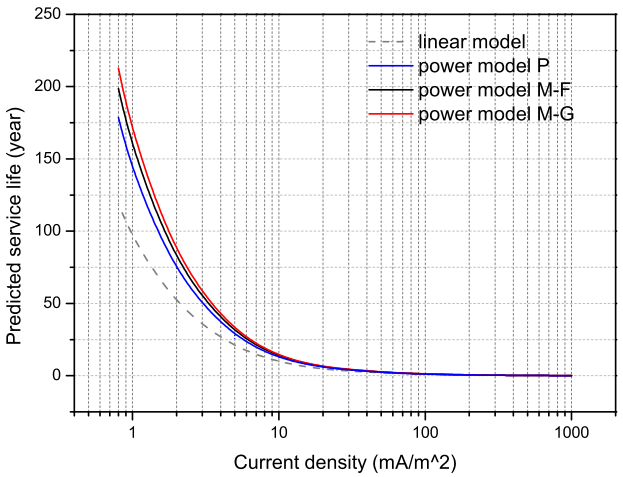

Figure 5.22: Predicted service life using the power model in comparison with the linear model.

5.5 Effect on the chloride threshold content

Figure 5.23 presents the chloride penetration profiles at different exposure times. The obtained fitted results of C_s and D_a are given in Table 5.7.

Figure 5.24 presents the monitored potential response and the calculated corrosion rate of selected specimens from each test group as an example. The complete data for the specimens were in Paper IV. Images of the steel surfaces of the respective specimens (except P-5j-B1, which is still under monitoring) are shown in Figure 5.25.

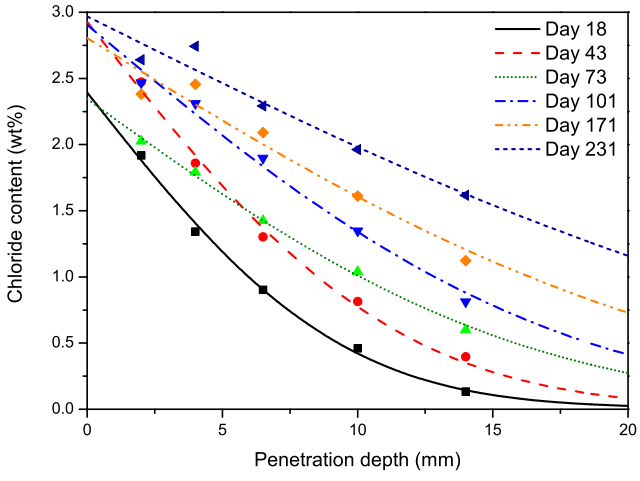

Figure 5.23: Chloride penetration profiles at different exposure times.

Specimens P-0j-A13 and P-0j-A14 represent two scenarios in the reference group. As an example, for P-0j-A14, the starting point of depassivation matched the increase in the corrosion rate, and thus the onset of corrosion was identified based on these two indicators. For the case of P-0j-A13, these two starting indicators did not match well. As can be seen in Figure 5.24a, the corrosion rate remained below 0.1 μA/m^2 while the depassivation started at day 14. The first corrosion rate monitored greater than 0.1 μA/m^2 was at day 75, which matched a depassivation/repassivation cycle that had started at day 74. Because the corrosion rate is a direct indicator, the onset of corrosion for the reference group was determined to be at day 74.

Table 5.8 summarizes the interpretation of the onset of corrosion for each specimen in the reference group. Depending on the different methods to calculate the average onset for the reference group, the corresponding chloride threshold content was also influenced, as shown in Table 5.9. However, the final result for the onset was chosen to be 55 days for the reference group, as indicated by the corrosion rate criterion.

For specimen P-1j-A1, although the 1-h decay was influenced by the power breakdown between day 82 and 83, it was quite stable and remained close to 50 mV until around day 112. It was noticeable that there was a small drop in both the polarization and 1-h depolarization curves around day 112, which may indicate the initiation of corrosion. Because there was a lack of corrosion rate data between day 83 and 180, the corrosion onset for P-1j-A1 was determined to be day 112, as this

Table 5.7: Results of C_s and D_a from regression analysis

Exposure time	C_s (wt%)	D_a (m^2/s)	R^2
Day 18	2.393	17.2×10^{-12}	0.997
Day 43	2.928	10.7×10^{-12}	0.995
Day 73	2.345	12.6×10^{-12}	0.997
Day 101	2.904	10.5×10^{-12}	0.987
Day 171	2.804	10.5×10^{-12}	0.947
Day 231	2.968	13.5×10^{-12}	0.945

Table 5.8: Interpretation of corrosion onset for the reference group

Specimen	Corrosion onset (day)	Criteria and remarks
P-0j-A10	11	depassivation; i_{cor} with uncertainty
P-0j-A11	2	depassivation and i_{cor}
P-0j-A12	8	depassivation and i_{cor}
P-0j-A13	14	depassivation
	74	i_{cor}
P-0j-A14	72	depassivation and i_{cor}
P-0j-A15	20	depassivation and i_{cor}

Table 5.9: Average corrosion onset of reference group and corresponding chloride threshold content at the cover depth

	$t_{\text{P-0j-A13}} = 74$ day		$t_{\text{P-0j-A13}} = 14$ day	
	Inc. all	&Exc. $t_{cor} < 2$w	Inc. all	&Exc. $t_{cor} < 2$w
Avg. $t_{cor-ref}$ (day)	31.2	55.3	21.2	35.3
C_{cr-ref} (wt%)	0.61	0.91	0.51	0.65

was on the conservative side.

Two examples from the 2 mA/m^2 group, P-2j-B11 and P-2j-B12, were selected to present briefly here. Specimen P-2j-B11 was found to have no corrosion until the termination of the experiment, based on all three criteria. Based on criteria (a) and (b), the corrosion onset for P-2j-B12 was determined to be around day 200, because it showed an OCP drop around the determined corrosion onset and the corrosion rate measurements were confirmed to be greater than 0.1 μA/m^2 as well.

Specimen P-5j-B1 was determined to have no corrosion occurring until the termination of the experiment, however, they were still being monitored and so not yet opened for visual inspection. Although one or two i_{cor} measurements were greater than 0.1 μA/m^2, the increase of i_{cor} was not consistent, and the following values went back to and remained at the safety level.

Table 5.10 summarizes the average results for the onset for each test group and their corresponding C_{cr} values. Under the prevention current densities of 1 mA/m^2 and 2 mA/m^2, the chloride threshold content was increased by 74% and 93%, compared to the reference group. There was no sign of corrosion observed under 5 mA/m^2 until the experiment was terminated, implying an increase in the chloride threshold value at least by double.

Table 5.10: Effect of cathodic prevention on chloride threshold content

Group	Specimen included	Avg. t_{cor} (day)	C_{cr} (wt%)	Increase
Reference	4	55	0.91	–
1 mA/m^2	3	154	1.58	74%
2 mA/m^2	4	190	1.76	93%
5 mA/m^2	2	> 265	> 2.03	> 124%

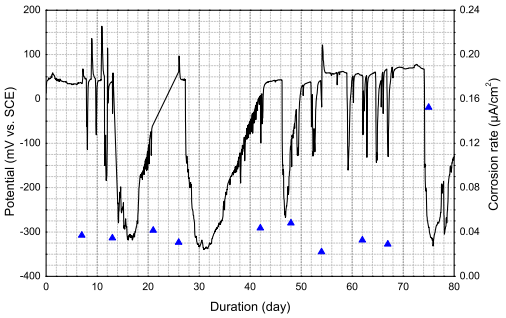

(a) Reference P-0j-A10

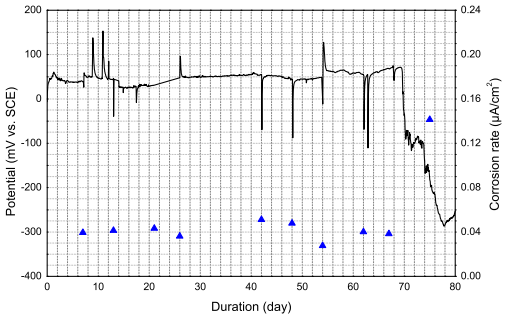

(b) Reference P-0j-A14

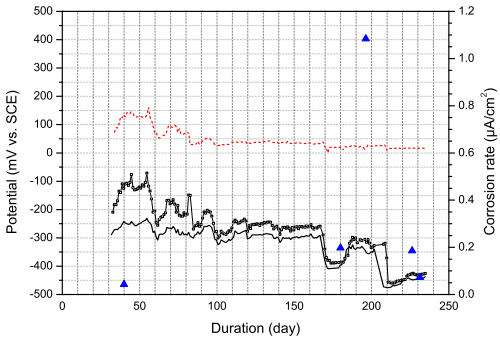

(c) P-1j-A3

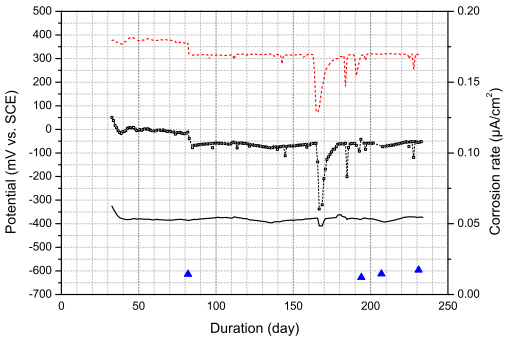

(d) P-2j-B10

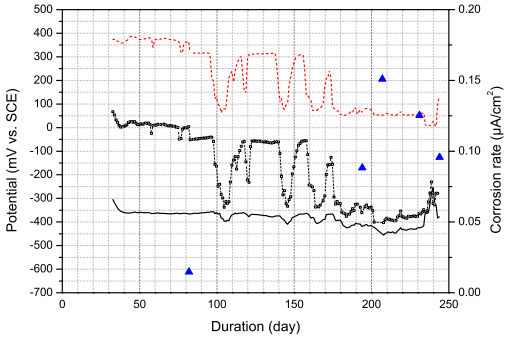

(e) P-2j-B14

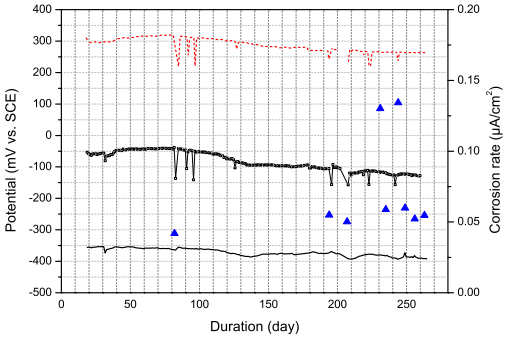

(f) P-5j-B1

Figure 5.24: Examples of corrosion monitoring from each test group. Solid lines are the steel potentials (vs. SCE). Corrosion rates are measured by cathodic polarization (▲). The complete data is presented in Paper IV.

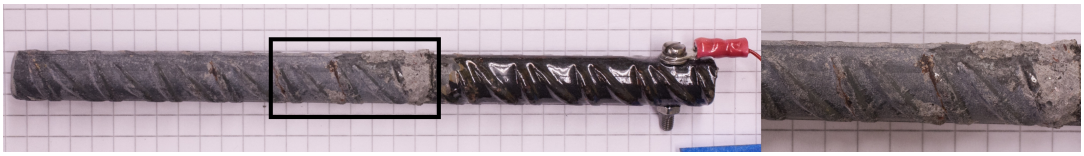

(a) P-0j-A13

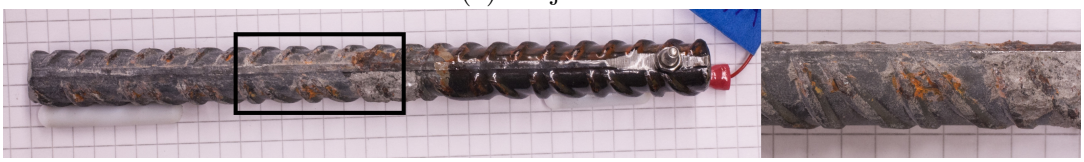

(b) P-0j-A14

(c) P-1j-A3

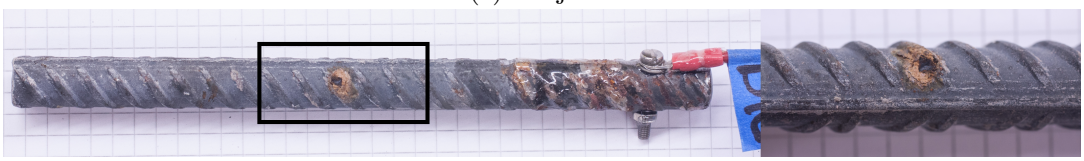

(d) P-2j-B10

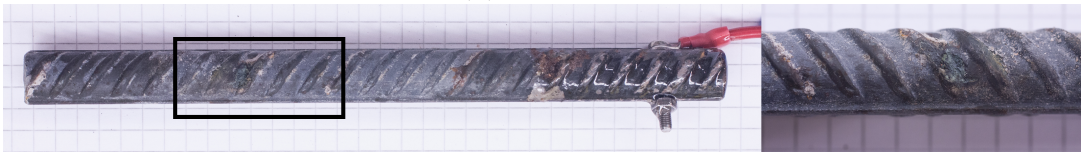

(e) P-2j-B14

Figure 5.25: Images of steel surface of selected specimens from each test group as examples. Zoom-in images of highlighted areas are on the right side.

5.6 Extended service life of ICCPre systems

By solving Equation 2.8 with a given C_{cr} value, the service life for a reinforced concrete structure against chloride initiated corrosion can be calculated. The input parameters are:

- $C_i = 0.01\%$ by mass of binder;
- $C_s = 3.1\%$ by mass of binder, for OPC conrete in tidal and splash zone, partial factor = 1, according to *DuraCrete*;
- $D_{\mathrm{RCM}} = 12.2 \times 10^{-12}$ m^2/s, for OPC concrete with a w/c ratio of 0.4, tested by the RCM test according to *NT Build 492* (Tang 2008);
- $n_{cl} = 0.37$, for OPC concrete in tidal and splash zone according to *DuraCrete*;

- $d = 40$ mm, based the common value for concrete cover discussed in Section 2.5.1.

Figure 5.26 shows the estimated service life when choosing different chloride threshold values using the DuraCrete model. Detailed data is given in Table 5.11. It can been seen that by imposing a current density of 2 mA/m^2, the service life became six times greater than for the reference group.

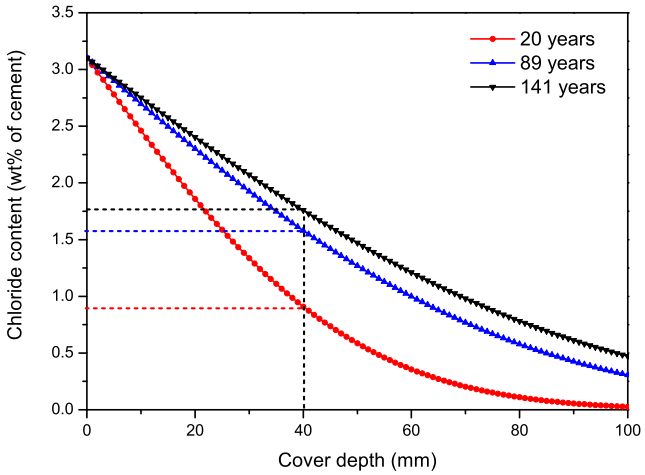

Figure 5.26: Estimated service life when using different chloride threshold values (cover depth = 40 mm)

Table 5.11: Service life of reinforced concrete using different chloride threshold contents (cover depth = 40 mm)

Current density	C_{cr} (wt%)	Calculated service life (years)	Increase
No current	0.91	20	–
1 mA/m^2	1.58	89	340%
2 mA/m^2	1.76	141	600%

Chapter 6

Conclusions

6.1 General conclusions

Based on the experimental results, the general conclusions can be summarized as follows.

- The carbon fiber embedded in the specimen remained undamaged under 4 A/m^2, although the polymer matrix was degraded due to oxidation, which implies that CFRP can be used as an anode material for ICCP applications.
- The degradation zone formed at the anode–concrete interface under ICCP was a consequence of the acid formation and calcium leaching caused by current exchange and chemical reactions, which led to an increase of resistivity and adhesion loss between the anode and the paste, and may eventually make the system fail due to the loss of protection efficiency.
- The degraded cement paste, to a large extent, constituted by branched and networked structures and the C-S-H gel, became polymerized or more amorphous, in which the w/c ratio was lowered. The maximum calcium leaching degree was found to be 80% of the original calcium content.
- The damage zone around the CFRP anode was strongly influenced by the current density and its distribution as well as the type of binder. The mortar specimens can tolerate more charge passage than the paste specimens. Moreover, between the two types of mortar binders, although their electrical behaviors were quite similar, the average leaching depths of M-G (with 25% GGBS) were smaller than those of M-F (with 20% fly ash), and the damage was less obvious for the M-G groups.
- A nonlinear conversion model was proposed to predict the service life of cathodic protection and prevention applications. Based on the acceleration factors obtained from the accelerated tests with three types of binder systems

at three different levels of current densities, the difference in the predicted service life between the nonlinear and linear models can be 30%–40% depending on the current density used in the protection or prevention system.

- Impressed cathodic currents even at low densities have shown a beneficial effect on increasing the chloride threshold content. Compared to the reference group, the chloride threshold content was increased by 74% under the current density of 1 mA/m^2 and 93% under 2 mA/m^2. There was no sign of corrosion observed under 5 mA/m^2 until the experiment was terminated, implying an increase in chloride threshold value by at least a factor of two.
- With 2 mA/m^2, the service life of reinforced concrete can be prolonged about three times more than that without cathodic prevention.

Regarding the testing methods that have been developed in this work, some additional conclusions can be drawn:

- An accelerated test method for ICCP was suitable for studying the chemical and microstructural changes at the anode–concrete interface and for investigating the damage pattern and service life of ICCP systems.
- The approach of determining the chloride threshold content by curve-fitting known chloride penetration profiles (at the same condition) was proven to be effective. The method for corrosivity monitoring with multi-indicators worked fairly well and the detected corrosion was confirmed by visual observation after the release of the rebar from the concrete specimen. Preconditioning of the specimens was useful to shorten the experimental time.
- It has also been proven that LA-ICP-MS is a reliable tool to analyze major and trace elements in the HCP and concrete materials.

Based on the experience from the experiment, it can be also suggested that more specimens (three to six) in one test group should be used in order to obtain an average value with more confidence and statistical support. It is better for the current density used in the accelerated tests to not exceed 1.5 A/m^2 of anode surface, if there are no special reasons or requirements, because extremely large current densities might lead to cable connection errors and other unexpected damage to the specimens.

6.2 Suggestions for future research

Due to limitations of time and resources, the conclusions of the accelerated model were drawn based on a limited number of specimens and a few variables. To further validate the conversion model, more testing data is needed to verify or modify the

model to better represent different testing conditions, such as current density level, binder type, w/c ratio, exposure conditions (chloride concentration, moisture, oxygen), and sizes of the specimens.

It still remains unclear what is the precise mechanism and model for the acid formation at the anode surface under ICCP. More experimental data is required to provide some key parameters for numerical modeling, such as the transference number, dissolution/precipitation rate, and pH. In parallel, a more sophisticated mathematical description of this complex process, combining both mass transport and chemical reactions, is much needed.

As there is a large variety of commercial CFRP materials available in the market, to be able to be widely used in practice, clear demands or specifications for CFRP as anode material should be made. A comprehensive and solid scientific proof of its functionality and durability is definitely required, such as to specify the limiting operating conditions (maximum applied voltage and current) and the service life under a given operating condition.

Regarding field applications, innovative cabling techniques for CFRP mesh anode are needed. Unlike metals, CFRP mesh anode can not be soldered or reshaped easily. Conventional cable connection methods may induce localized resistance to the CFRP anode–cable interface that could cause corrosion problems for the cables. To prevent this type of connection problem and make the CFRP anode easy to handle, innovative cabling techniques, such as utilizing conductive mortar as a bridging unit, will benefit the wide application of CFRP as anode material in ICCP systems.

Long-term field tests are of great interest to investigate the overall functionality and durability of CFRP anode and ICCPre systems as a whole. However, this is also a great challenge, considering that the time-span of such investigation could easily last for more than ten years and require continuous efforts for data acquisition, documentation, and analysis.

Regarding pitting-corrosion related durability design, the beneficial effect of cathodic prevention technique should be considered, perhaps in coooperation with a delayed energizing of the system to reach the goal of extending the service life and optimizing the energy cost. Current density related and depolarization related criteria should be also used as protection criteria.

Smart corrosion monitoring techniques and tools also need to be further developed, in order to give reliable testing results and better adjust or predict the maintenance plan, as well as reduce the manual operation time.

Bibliography

AASHTO T 260-97. Standard Method of Test for Sampling, Testing for Chloride Ion in Concrete, and Concrete Raw Materials (cit. on pp. 7, 36).

Ahmad, Shamsad (2003). "Reinforcement corrosion in concrete structures, its monitoring and service life prediction — A review". In: *Cement and Concrete Composites* 25.4. Concrete Durability, pp. 459–471 (cit. on p. 8).

Ali, Mohammad Golam, Rasheeduzzafar, and S. S. Al-Saadoun (1992). "Migration of ions in concrete due to cathodic protection current". In: *Cement and Concrete Research* 22.1, pp. 79–94 (cit. on p. 19).

Andrade, C (2002). *Analysis of total chloride content in concrete*. Tech. rep. 9. RILEM TC 178-TMC: Testing and Modelling Chloride Penetration in Concrete, pp. 583–585 (cit. on p. 7).

Andrade, C, R Cigna, R Nurnberger, R Polder, R Weydert, and E Seitz (2003). "Corrosion state monitoring". In: *Corrosion of steel in reinforced concrete structure, COST Action* 521, pp. 101–111 (cit. on p. 7).

Angst, Ueli, Bernhard Elsener, Claus K. Larsen, and Øystein Vennesland (2009). "Critical chloride content in reinforced concrete — A review". In: *Cement and Concrete Research* 39.12, pp. 1122–1138 (cit. on p. 7).

ASTM C1152/C1152M. Standard Test Method for Acid-Soluble Chloride in Mortar and Concrete (cit. on p. 7).

ASTM C876-15. Standard Test Method for Corrosion Potentials of Uncoated Reinforcing Steel in Concrete (cit. on p. 8).

Atkins, Chris P., David M. Wright, and Paul Lambert (2017). "Assessment of the depolarization of cathodically protected reinforced concrete". In: *Materials and Corrosion* (cit. on p. 12).

Babaahmadi, Arezou (2015). "Durability of cementitious materials in long-term contact with water". PhD thesis. Chalmers University of Technology (cit. on p. 45).

Bahekar, Prasad V. and Sangeeta S. Gadve (2017). "Impressed current cathodic protection of rebar in concrete using Carbon FRP laminate". In: *Construction and Building Materials* 156, pp. 242–251 (cit. on p. 12).

Bertolini, L, F Bolzoni, P Pedeferri, L Lazzari, and T Pastore (1998). "Cathodic protection and cathodic preventionin concrete: Principles and applications". In: *Journal of Applied Electrochemistry* 28.12, pp. 1321–1331 (cit. on p. 9).

Bertolini, L., F. Bolzoni, M. Gastaldi, T. Pastore, P. Pedeferri, and E. Redaelli (2009). "Effects of cathodic prevention on the chloride threshold for steel corrosion in concrete". In: *Electrochimica Acta* 54.5, pp. 1452–1463 (cit. on pp. 10, 12, 15).

Bertolini, Luca, Fabio Bolzoni, Tommaso Pastore, and Pietro Pedeferri (2004). "Effectiveness of a conductive cementitious mortar anode for cathodic protection of steel in concrete". In: *Cement and Concrete Research* 34.4, pp. 681–694 (cit. on pp. 12, 14, 16).

Bertolini, Luca, Bernhard Elsener, Pietro Pedeferri, Elena Redaelli, and Rob B Polder (2013). "Corrosion of Steel in Concrete: Pprevention, Diagnosis, Repair". In: WILEY-VCH. Chap. Electrochemical aspects, pp. 109–124 (cit. on p. 5).

Boubitsas, Dimitrios and Luping Tang (2013). "An approach for measurement of chloride threshold values". In: *International Journal of Structural Engineering* 4, pp. 24–34 (cit. on p. 36).

Brown, P. W. and J. R. Clifton (1988). "Mechanisms of deterioration in cement-based materials and in lime mortar". In: *Durability of Building Materials* 5, pp. 409–420 (cit. on p. 11).

Chaussadent, T. and G. Arliguie (1999). "AFREM test procedures concerning chlorides in concrete: Extraction and titration methods". In: *Materials and Structures* 32.3, pp. 230–234 (cit. on p. 7).

Chen, Wei (2006). "Hydration of slag cement: Theory, modeling and application". PhD thesis. University of Twente (cit. on p. 40).

Climent, Miguel A., Estanislao Viqueira, Guillem de Vera, and M.M. López-Atalaya (1999). "Analysis of acid-soluble chloride in cement, mortar, and concrete by potentiometric titration without filtration steps". In: *Cement and Concrete Research* 29.6, pp. 893 –898 (cit. on p. 7).

Cong, Xiandong and R. James Kirkpatrick (1996). "29Si MAS NMR study of the structure of calcium silicate hydrate". In: *Advanced Cement Based Materials* 3, pp. 144–156 (cit. on p. 47).

Cramer, S. D., B. S. Covino, G. R. Holcomb, S. J. Bullard, W. K. Collins, R. D. Govier, R. D. Wilson, and H. M. Laylor (1999). "Thermal sprayed titanium anode for cathodic protection of reinforced concrete bridges". In: *Journal of Thermal Spray Technology* 8.1, pp. 133–145 (cit. on p. 11).

Darowicki, K., J. Orlikowski, S. Cebulski, and S. Krakowiak (2003). "Conducting coatings as anodes in cathodic protection". In: *Progress in Organic Coatings* 46.3, pp. 191–196 (cit. on p. 16).

Daube, J. and R. Bakker (1986). *Portland Blast-Furnace Slag Cement: A Review.* Tech. rep. ASTM International, West Conshohocken, PA, (cit. on p. 40).

Davies, Kevin and John Broomfield (2013). "Cathodic Protection of Steel in Concrete and Masonry". In: ed. by and John P. Broomfield Paul M. Chess. 2nd. CRC Press Boca Raton, FL. Chap. Cathodic protection mechanism and a review of criteria, pp. 41–56 (cit. on p. 9).

Dhir, R.K., M.R. Jones, and H.E.H. Ahmed (1990). "Determination of total and soluble chlorides in concrete". In: *Cement and Concrete Research* 20.4, pp. 579–590 (cit. on p. 7).

Dreyman, Edgar W (1972). "Precious metal anodes – State of art". In: *Materials Protection and Performance* 11.9, p. 17 (cit. on p. 16).

Eichler, T., B. Isecke, G. Wilsch, S. Goldschmidt, and M. Bruns (2010). "Investigations on the chloride migration in consequence of cathodic polarisation". In: *Materials and Corrosion* 61.6, pp. 512–517 (cit. on pp. 13, 14).

Engelund, S, C Edvardsen, and L Mohr (2000). *General guidelines for durability design and redesign*. Report R15 of EU-Brite EuRam III project BE95-1347 DuraCrete. Probabilistic performance based durability design of concrete structures (cit. on pp. 17, 58).

Eurocode 2 (1992). Design of concrete structures (cit. on p. 18).

Glass, Gareth K, Alaa M Hassanein, and Nick R Buenfeld (2000). "CP criteria for reinforced concrete in marine exposure zones". In: *Journal of materials in civil engineering* 12.2, pp. 164–171 (cit. on p. 12).

Glass, G.K. and J.R. Chadwick (1994). "An investigation into the mechanisms of protection afforded by a cathodic current and the implications for advances in the field of cathodic protection". In: *Corrosion Science* 36.12, pp. 2193–2209 (cit. on p. 12).

Glass, GK, AM Hassanein, and NR Buenfeld (2001). "Cathodic protection afforded by an intermittent current applied to reinforced concrete". In: *Corrosion Science* 43.6, pp. 1111–1131 (cit. on p. 13).

Heidersbach, R.H., J. Brandt, D. Johnson, J.S. Smart III, and J.S. Smart (2006). "Marine Cathodic Protection, ASM Handbook". In: vol. 13C. ASM International. Chap. Corrosion: Environments and Industries, pp. 73–78 (cit. on p. 16).

Hendy, C.R. and D.A. Smith (2007). "Durability and cover to reinforcement". In: *Designers' Guide to EN 1992-2 Eurocode 2 - Design of Concrete Structures, Part 2: Concrete Bridges*. ICE Publishing. Chap. 4, pp. 31–38 (cit. on p. 18).

Henriksen, J.F. (1980). "The corrosion and protection of steel in saturated Ca(OH)2 contaminated with NaCl". In: *Corrosion Science* 20.11, pp. 1241–1249 (cit. on p. 12).

Hoar, T.P. (1967). "On the relation between corrosion rate and polarization resistance". In: *Corrosion Science* 7.7, pp. 455–458 (cit. on p. 13).

Hoar, T.P. and W.R. Jacob (1967). "Breakdown of passivity of stainless steel by halide ions". In: *Nature* 216.5122, p. 1299 (cit. on p. 6).

Hoar, T.P., D.C. Mears, and G.P. Rothwell (1965). "The relationships between anodic passivity, brightening and pitting". In: *Corrosion Science* 5.4, pp. 279–289 (cit. on p. 5).

ISO-12696 (2012). *Cathodic Protection of Steel in Concrete* (cit. on pp. 10, 11, 17).

Jing, Xu and Yao Wu (2011). "Electrochemical studies on the performance of conductive overlay material in cathodic protection of reinforced concrete". In: *Construction and Building Materials* 25.5, pp. 2655–2662 (cit. on p. 16).

Jochum, Klaus Peter, Ulrike Weis, Brigitte Stoll, Dmitry Kuzmin, Qichao Yang, Ingrid Raczek, Dorrit E Jacob, Andreas Stracke, Karin Birbaum, and Daniel A Frick (2011). "Determination of reference values for NIST SRM 610–617 glasses following ISO guidelines". In: *Geostandards and Geoanalytical Research* 35.4, pp. 397–429 (cit. on p. 32).

Kessler, Rechard J and Rodney G Powers (1989). "Conductive rubber as an impressed current anode: cathodic protection of steel-reinforced concrete". In: *Materials performance* 28.9, pp. 24–27 (cit. on p. 16).

Kim, Jung J., Muhammad K. Rahman, and Mahmoud M. Reda Taha (2012). "Examining microstructural composition of hardened cement paste cured under high temperature and pressure using nanoindentation and 29Si MAS NMR". In: *Applied Nanoscience* 2.4, pp. 445–456 (cit. on p. 32).

Koster, T., W. Peelen, J. Larbi, M. de Rooij, and R. Polder (2010). "Numerical model of $Ca(OH)_2$ transport in concrete due to electrical currents". In: *Materials and Corrosion* 61.6, pp. 518–523 (cit. on p. 15).

Küter, Andre (2009). "Management of Reinforcement Corrosion: A Thermodynamic Approach". PhD thesis. Technical University of Denmark (DTU) (cit. on p. 5).

Kurumisawa, Kiyofumi, Toyoharu Nawa, Hitoshi Owada, and Masahito Shibata (2013). "Deteriorated hardened cement paste structure analyzed by XPS and 29Si NMR techniques". In: *Cement and Concrete Research* 52.10, pp. 190–195 (cit. on pp. 32, 47).

Lambert, Paul, Chinh Van Nguyen, Pritpal S Mangat, Finbar J O'Flaherty, and Graeme Jones (2015). "Dual function carbon fibre fabric strengthening and impressed current cathodic protection (ICCP) anode for reinforced concrete structures". In: *Materials and Structures* 48.7, pp. 2157–2167 (cit. on p. 17).

Le Saoût, Gwenn, Eric Lécolier, Alain Rivereau, and Hélène Zanni (2006). "Chemical structure of cement aged at normal and elevated temperatures and pressures, Part II: Low permeability class G oilwell cement". In: *Cement and Concrete Research* 36.3, pp. 428–433 (cit. on p. 32).

Mahdi, Chini (2010). "Pan-based carbon fiber as anode material in cathodic protection systems for concrete structures". PhD thesis. Norwegian University of Science and Technology (cit. on p. 16).

Matsushita, Fumiaki, Yoshimichi Aono, and Sumio Shibata (2004). "Calcium silicate structure and carbonation shrinkage of a tobermorite-based material". In: *Cement and Concrete Research* 34.7, pp. 1251–1257 (cit. on p. 32).

Mayer, S. (2004). "Cathodic protection investigations into the effectiveness of a cathodic protection system for reinforced concrete specimens in order to optimize anode fields". PhD thesis. Munich university of applied science (cit. on p. 16).

Mietz, J, J Fischer, and B Isecke (2001). "Cathodic protection of steel-reinforced concrete structures – Results from 15 years' experience". In: *Materials Performance* 40.12, pp. 22–26 (cit. on pp. 13, 14, 19).

Mork, J.H., S. Mayer, and K. Rosenbom (2006). "Cathodic protection of concrete structures with a carbon fiber mesh anode". In: *EUROCORR2006*. Maastricht, the Netherlands (cit. on pp. 16, 17).

Mork, J.H., S. Mayer, and R. Asheim (2007). "The performance of cathodic protection on harbor and jetty of Honningsvåg Norway". In: *Proceeding of the 5th International Conference on Concrete Structures Under Extreme Conditions of Environment and Loading, CONSEC'07, Tours, 4-6 June 2007*. Vol. 1 (cit. on p. 17).

Morris, W., A. Vico, M. Vazquez, and S. R. de Sanchez (2002). "Corrosion of reinforcing steel evaluated by means of concrete resistivity measurements". In: *Corrosion Science* 44.1, pp. 81–99 (cit. on p. 35).

NACE (2007). *Impressed current cathodic protection of reinforcing steel in atmospherically exposed concrete structures* (cit. on p. 28).

Newman, John and Karen E Thomas-Alyea (2012). *Electrochemical systems*. 3rd edition. John Wiley & Sons (cit. on p. 11).

Newton, C.J and J.M Sykes (1988). "A galvanostatic pulse technique for investigation of steel corrosion in concrete". In: *Corrosion Science* 28.11, pp. 1051–1074 (cit. on p. 34).

Nguyen, C. V., P. S. Mangat, P. Lambert, F. J. O' Flaherty, and G. Jones (2012a). "Dual function carbon fibre strengthening and cathodic protection anode for reinforced concrete structures". In: *Concrete Repair, Rehabilitation and Retrofitting III*. CRC Press, pp. 1179–1185 (cit. on p. 17).

Nguyen, Chinh Van, Paul Lambert, Pal Mangat, Fin O'Flaherty, and Graeme Jones (2012b). "The performance of carbon fibre composites as iccp anodes for reinforced concrete structures". In: *ISRN Corrosion* (cit. on p. 17).

NT Build 492. Concrete, mortar and cement-based repair materials: chloride migration coefficient from non-steady-state migration experiments (cit. on pp. 18, 58).

Pech-Canul, M.A and P Castro (2002). "Corrosion measurements of steel reinforcement in concrete exposed to a tropical marine atmosphere". In: *Cement and Concrete Research* 32.3, pp. 491–498 (cit. on p. 35).

Pedeferri, Pietro (1996). "Cathodic protection and cathodic prevention". In: *Construction and Building Materials* 10.5, pp. 391–402 (cit. on pp. 13, 14).

Peelen, W.H.A., R.B. Polder, and L. Redaelli E.and Bertolini (2008). "Qualitative model of concrete acidification due to cathodic protection". In: *Materials and corrosion* 59.2, pp. 81–89 (cit. on pp. 13, 15).

Polder, R. B., W. H. A. Peelen, B. Th. J. Stoop, and E. A. C. Neeft (2011). "Early stage beneficial effects of cathodic protection in concrete structures". In: *Materials and Corrosion* 62.2, pp. 105–110 (cit. on p. 15).

Polder, R. B., G. Leegwater, D. Worm, and W. Courage (2014). "Service life and life cycle cost modelling of cathodic protection systems for concrete structures". In: *Cement and Concrete Composites* 47, pp. 69–74 (cit. on pp. 13, 14, 19).

Polder, R.B. and W.H.A. Peelen (2011). "Service life aspects of cathodic protection of concrete structures". In: *Concrete Repair*. CRC Press, pp. 117–136 (cit. on pp. 14, 17, 45).

Polder, R.B., T.G. Nijland, W.H.A. Peelen, and L. Bertolini (2002). "Acid formation in the anode/concrete interface of activated titanium cathodic protection systems for reinforced concrete and the implications for service life". In: *15th International Corrosion Congress (ICC), Granada, Spain, September* (cit. on pp. 14, 39).

Proverbio, Edoardo and Fabio Carassiti (1997). "Evaluation of chloride content in concrete by X-ray fluorescence". In: *Cement and Concrete Research* 27.8, pp. 1213–1223 (cit. on p. 7).

Richardson, I. G. (1999). "The nature of C-S-H in hardened cements". In: *Cement and Concrete Research* 29.8, pp. 1131–1147 (cit. on p. 32).

Saito, Hiroshi and Akira Deguchi (2000). "Leaching tests on different mortars using accelerated electrochemical method". In: *Cement and Concrete Research* 30.11, pp. 1815–1825 (cit. on p. 11).

Samson, E., J. Marchand, and J.J. Beaudoin (2000). "Modeling the influence of chemical reactions on the mechanisms of ionic transport in porous materials: An overview". In: *Cement and Concrete Research* 30.12, pp. 1895–1902 (cit. on p. 15).

Sato, N. (1971). "A theory for breakdown of anodic oxide films on metals". In: *Electrochimica Acta* 16.10, pp. 1683–1692 (cit. on p. 6).

Schießl, P. and M. Raupach (1990). "Influence of concrete composition and microlimate on the critical chloride content in concrete". en. In: *Third International Symposium on Corrosion of Reinforcement in Concrete Construction* (cit. on p. 7).

Silva, Nelson (2013). "Chloride induced corrosion of reinforcement steel in concrete-Threshold values and ion distributions at the concrete-steel interface". PhD thesis. Chalmers University of Technology (cit. on pp. 6, 7).

Strehblow, H-H. and P. Marcus (2012). "Corrosion mechanisms in theory and practice". In: ed. by Philippe Marcus. 3rd. CRC Press. Chap. Mechanisms of pitting corrosion, pp. 349–391 (cit. on p. 5).

Sun, Hongfang, Guanping Guo, Shazim Ali Memon, Weiting Xu, Qiwu Zhang, Ji-Hua Zhu, and Feng Xing (2015). "Recycling of carbon fibers from carbon fiber reinforced polymer using electrochemical method". In: *Composites Part A: Applied Science and Manufacturing* 78, pp. 10–17 (cit. on p. 17).

Sun, Hongfang, Liangliang Wei, Miaochang Zhu, Ningxu Han, Ji-Hua Zhu, and Feng Xing (2016a). "Corrosion behavior of carbon fiber reinforced polymer anode in simulated impressed current cathodic protection system with 3% NaCl solution". In: *Construction and Building Materials* 112, pp. 538–546 (cit. on p. 17).

Sun, Hongfang, Shazim Ali Memon, Yang Gu, Miaochang Zhu, Ji-Hua Zhu, and Feng Xing (2016b). "Degradation of carbon fiber reinforced polymer from cathodic protection process on exposure to NaOH and simulated pore water solutions". In: *Materials and Structures* 49.12, pp. 5273–5283 (cit. on p. 17).

Tang, L. and P. Utgenannt (2009). "A field study of critical chloride content in reinforced concrete with blended binder". In: *Materials and Corrosion* 60.8, pp. 617–622 (cit. on p. 18).

Tang, Luping (2008). "Engineering expression of the ClinConc model for prediction of free and total chloride ingress in submerged marine concrete". In: *Cement and Concrete Research* 38.8-9, pp. 1092–1097 (cit. on pp. 18, 58).

Tang, Luping and Ying Fu (2006). "A rapid technique using handheld instrument for mapping corrosion of steel in reinforced concrete". In: *Restoration of Buildings and Monuments* 12.5-6, pp. 387–400 (cit. on p. 8).

Tang, Luping, Emma Qingnan Zhang, Ying Fu, Björn Schouenborg, and Jan Erik Lindqvist (2012). "Covercrete with hybrid functions — A novel approach

to durable reinforced concrete structures". In: *Materials and Corrosion* 63.12, pp. 1119–1126 (cit. on pp. 15, 17).

Zebger, Ingo, Aitziber Lopez Elorza, Javier Salado, Ainara Garcia Alcala, Elsa Silva Gonçalves, and Peter R. Ogilby (2005). "Degradation of poly(1,4-phenylene sulfide) on exposure to chlorinated water". In: *Polymer Degradation and Stability* 90.1, pp. 67–77 (cit. on p. 11).

Zhu, Ji-Hua, Liangliang Wei, Miaochang Zhu, Hongfang Sun, Luping Tang, and Feng Xing (2015). "Polarization Induced Deterioration of Reinforced Concrete with CFRP Anode". In: *Materials* 8.7, pp. 4316–4331 (cit. on p. 17).

Zhu, Ji-Hua, Liangliang Wei, Zhaohua Wang, Cheng Ke Liang, Yuan Fang, and Feng Xing (2016a). "Application of carbon-fiber-reinforced polymer anode in electrochemical chloride extraction of steel-reinforced concrete". In: *Construction and Building Materials* 120, pp. 275–283 (cit. on p. 17).

Zhu, Ji-Hua, Guanping Guo, Liangliang Wei, Miaochang Zhu, and Xianchuan Chen (2016b). "Dual Function Behavior of Carbon Fiber-Reinforced Polymer in Simulated Pore Solution". In: *Materials* 9.2, p. 103 (cit. on p. 17).